Escola de Camins
Escola Tècnica Superior d'Enginyeria de Camins, Canals i Ports
UPC BARCELONATECH

TREBALL FINAL DE MÀSTER

Development of a tool for a 2-phase flow Electrical Resistance Tomography image reconstruction and analysis

Treball realitzat per:
Gemma García Farrés

Dirigit per:
Antonio Rodríguez Ferran
Václav Matoušek

Màster en:
Enginyeria de Camins, Canals i Ports

Barcelona, 15 de juny de 2018

Departament d'Enginyeria Civil i Ambiental

Abstract

Slurry pipes usually contain a mixture of liquid and solid particles. The mixture of the water with the fine mass, gives as a result a non-Newtonian fluid. This non-Newtonian becomes a fluid carrier for the rest of the coarse particles giving, as a result, a two-phase flow (fluid-solid) which behaviour depends on the properties of the elements and the characteristics of the flow itself.

This work is based on the research into using Electrical Resistivity Tomography (ERT) as measurement technique to characterize a two-phase flow of non-Newtonian fluid and solid particles, in order to better understand the functioning of a slurry pipe. ERT is a current injection based method that maps voltages obtained inside a domain, in this case of study the cross section of the pipe. With this voltages, an image can be reconstructed and so, by associating this values with concentration, some useful data can be inferred.

For thus, it is set up a tool able to reconstruct the raw images collected by the ERT system with an accurate performance and reliability. Once this tool is set up, 2D local concentration distribution, 1D concentration profiles and average concentration of the cross-section for a two-phase flow are analysed and discussed, using different tests done with the ERT technique and other data collected with other methods such as video images or the velocity.

The results obtained are promising and give information enough to be used in the study of the two-phase mixture with a non-Newtonian fluid and a solid. With further adjustment of the script developed, the ERT plus the computational post-processing of the images designed may turn out to be a very powerful tool, for the different advantages that supposes over other imaging techniques in the slurry pipelines field.

Key words: *Electrical Resistivity Tomography, two-phase flow, non-Newtonian fluids, slurry pipelines.*

List of contents

List of Figures

List of tables

Introduction

Slurry pipelines (Figure 0.1) are used in the industrial sector to move ores, for example of coal or iron, and also tailings (mining waste). Slurry is considered to be the mixture of water and the ore concentrate, and is usually pumped to its destination where then, water and ore are separated. Pipeline hydraulic transport has been considered a progressive technology for conveying great quantities of these bulk materials since they have different kind of advantages compared to other kinds of mechanical transport (i.e. railroad transport) some of them are: the economic impact, less disturbance noise, substantially less space compared to other methods, dust free environment and that it might not need human intervention, except for the operating stuff (full automation).

Figure 0.1 Slurry pipeline. Source: (Banner Engineering).

If the concentration of fines in this transported mixture with water is high these slurries show non-Newtonian behaviour. When this happens, it is also important to know whether if the existing coarse particles are suspended in the non-Newtonian carrier or they settle down (Kesely & Matoušek, Laminar Settling Of Glass Beads In Visco-Plastic Liquids, 2016). Moreover, the construction, design and operation of this pipeline has a higher complexity due to the nature of the slurry.

For this purpose, experiments on two-phase flows with non-Newtonian fluids have been carried out to improve the knowledge on their behaviour for the past years. Henceforth, the aim of this master thesis is to create a tool that post-processes the images obtained with the use a non-invasive obtaining of images in a pressurized pipe where a non-Newtonian fluid with coarse particles is pumped, and analyse the values obtained from the post-process and interpretation of the images. More specifically, this improvements have the goal of providing information over the distribution and concentration of this coarse

particles inside the pipe which can be further related with other hydraulic parameters, and subsequently, give a better comprehension of the behaviour of a multiphase flow with a non-Newtonian fluid and a carrying solid.

The imaging technique used for this non-intrusive data collection is Electrical Resistance Tomography (ERT). In ERT, current is injected into and removed from the pipe by paired electrodes. The resulting voltage is measured between the remaining electrode pairs. ERT maps these boundary voltages into a conductivity distribution that represents the domain of the pipe. For so, this technique can provide significant information in the case of opaque objects.

ERT, or in its defect EIT or ECT (Electrical Impedance or Capacitance Tomography), is used in various fields (i.e. medical scans, hydraulics, geophysics) for its non-invasive functionality and its low cost compared to other techniques, like X-ray system. With further development in computer engineering it can be expected that electrical tomography will become faster and more accurate, so that its use will become more popular for its benefits in comparison with other techniques.

The processing of the image obtained with the ERT system is done by a set of open-source scripts, EIDORS, which works on a finite element method ill-posed problem and tries to approximate the conductivity changes to obtain the best fitting images. As the problem is an ill-posed problem, the numerical solution tends to be unstable and has to be really well conditioned which has also become part of this work.

Once the images have been processed the values for this finite element field can be extrapolated to concentrations describing 2D local concentration distribution maps, allowing to calculate average concentrations along the vertical axis of the pipe and mean average concentrations in a specific cross-section, and all these values and can be related with other known physical parameters.

This document serves as summary where, first of all, it has been introduced the reader to the topic of study with an initial brief description of the properties of the non-Newtonian fluids, the two-phase flow and the imaging technique, ERT. Afterwards, an explanation of the objectives developed during this work, and the methodology followed to reach them, has been explained. Henceforward, presentation and discussion of the results obtained are shown and, finally, the conclusions drawn from this work are presented.

Chapter 1. State of art

First of all, it is important to comprehend the characteristics of the behaviour of this slurry pipes which makes them different from the pressurised water (Newtonian characteristics) pipelines transporting solid particles. Therefore, it is important to understand which one is the difference between a Newtonian and a non-Newtonian fluid. Furthermore, it is explained also the kind of flow generated when this two phases, solid and non-Newtonian, are mixed together.

In the same way, a brief description of the working method used in the laboratory in order to obtain the images is explained: Electrical Resistivity Tomography. Although the main subject of this work is not the development of the method, it is included in this chapter in order to better understand the technique that is used in this work to obtain the data that it is further post-processed and analysed for the study of the two-phase flow.

Also, the main characteristics of the image visualization tool which is used for the post-process of the raw imaging data, EIDORS, are explained in this chapter.

1.1 Non-Newtonian fluids

Frequently, the variables used to describe a fluid flow are its density, velocity, pressure and stresses. The constitutive relation between the stress and the strain rate is based on rheological models. Analysing the incompressible fluids response under shear rate and shear stress we can divide the fluid into Newtonians and non-Newtonians. The constitutive model for a fluid is usually well described by Newton's law of viscosity,

$$\tau = \mu \frac{du}{dy} \quad \textbf{(1)}$$

where τ the shear stress (Pa), μ dynamic viscosity (Pa·s), and du/dy (1/s) is the shear rate.

All the fluids following this linear relation are called Newtonian fluids. The Newton's law describes a fluid with the next characteristics:

1. The viscosity is independent of the shear rate.
2. The viscosity is independent of time of shear at a constant shear rate.
3. The normal stress differences are zero.
4. The viscosities measured by different types of deformations, such as uniaxial and biaxial extension, are proportional to each other.

This law states that the rate of deformation an element volume of the fluid suffer is proportional to stress. If Newton's law is not is not obeyed, and the relationship between the stress and the deformation is more complex the fluid is called a non-

Newtonian. In other words, a non-Newtonian fluid is one whose flow curve shows an apparent viscosity that depends on flow conditions such as flow geometry, shear rate, etc. and sometimes even on the kinematic history of the fluid element under consideration. Depending on the relation of proportion between the shear stress and the velocity gradient, several types of Non-Newtonian can be described (Figure 1.1):

- Shear thinning (visco-elastic): viscosity decreases with increasing velocity gradient (polymers, glues, wall paints, etc.).
- Shear thickening (dilatant): viscosity increases with increasing velocity gradient (solvents, starch grout, concrete, etc.).
- Pseudo-plastic: The yield stress, τ_y, has to be overcome to turn the fluid into motion (chocolate, syrups, sludge, etc.).
- Rheopectic: Viscosity increases with duration of stress (printer ink, gypsum paste, etc.).
- Thixotropic: Viscosity decreases with the duration of stress (yogurt, many paints, many gels, etc.).

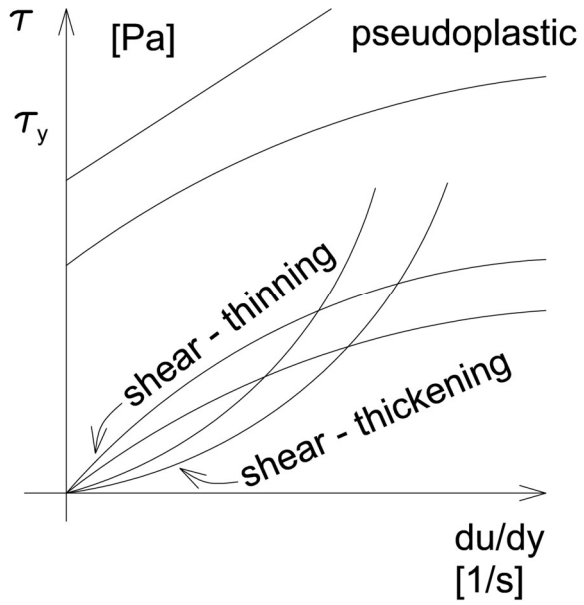

Figure 1.1 Rheological classification for non-Newtonian fluids. Source: (Kesely, 2016).

Most of the non-Newtonian fluids are shear thinning or ‘pseudo plastic’. That means that viscosity decreases as the strain rate is increased. At very low shear rates, usually the viscosity value behaves as a constant value. As the shear rate is increased there is a decrease in the viscosity, and the viscosity once again tends to another constant lower value.

Herschel-Bulkley fluids are pseudo plastic fluids which also have to overcome and initial yield stress. The law defining this kinds of fluid corresponds to:

$$\tau = \tau_y + K\left(\frac{du}{dy}\right)^n \quad \textbf{(2)}$$

where τ is the shear stress, τ_Y is yield stress to overcome and K consistency index, and n is the flow index and defines the shear thickening($n>1$) or thinning ($0<n<1$). Figure 1.2 shows this behaviour.

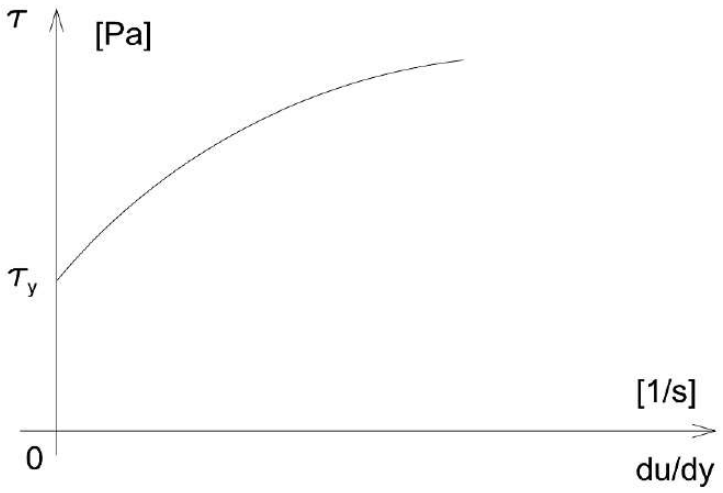

Figure 1.2 Rheological behaviour of a Herschel-Bulkley fluid. Source: (Kesely, 2016).

1.2 Multiphase flows

Slurry flows are not only described by the non-Newtonian fluids behaviour but also by the coarse particles transported, which can settle in the bottom or float in the cross-section of the pipe. For thus, it is important also to describe the flow generated by the non-Newtonian fluid and the solids that is carrying.

Generally, a carrying liquid may flow either in laminar or a turbulent regime in a pipeline. A laminar flow is composed of thin layers (lamina) that move over each other at different velocities forming a typical parabolic velocity profile in a pipeline cross section (Figure 1.3). There is no exchange of mass and momentum between neighbouring layers. Thus each liquid particle has zero velocity components in directions other than the one direction following the direction of the main flow.

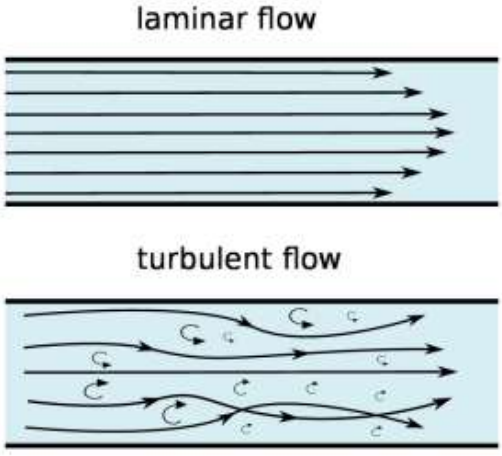

Figure 1.3 Streamlines in a laminar flow and a turbulent flow. Source: (CFD support).

This laminar regime can hardly occur when the carrying liquid is water (TU Delft OpenCourseWare, 2018). On the other hand, when the carrying liquid has higher viscosity, this laminar flow can be maintained at higher velocities. This is the case for the slurries, where high concentration of non-settling solid particles (fine fraction) are mixed with water.

However, in practice, the operational velocities of this pipelines are higher than the threshold velocity for laminar flow. When this happens, there is a turbulent flow. Turbulent flow can be described as a disturbance between layers, and for thus, turbulent eddies are generated (Figure 1.3). This eddies are the agents for severe random exchange of mass and momentum in all directions. Furthermore, this eddies are responsible for additional dissipation of energy, a part from the friction losses of the laminar flow.

Solid particles carried in the flow of a liquid are the main indicators of a pattern flow. The mixture flow is considered fully stratified if the intensity of turbulence of

the carrier fluid is not sufficient to suspend any solid particle in the pipeline and a granular bed appears in the bottom of the pipeline. The opposite extreme occurs when all solid particles are suspended within the stream. Consequently, a fully-suspended flow is considered. A mixture flow exhibits a considerable concentration gradient across a pipeline cross section indicating an accumulation of a portion of solids near the bottom of a pipeline and a non-uniform distribution of the rest of solids across the rest of the pipeline cross-sectional area. This pattern is known as heterogeneous flow or partially stratified. The fully-suspended flow may be considered pseudo-homogeneous if a distribution of solid particles across a transversal section of a stream is almost uniform.

In literature different flow patterns or flow regimes are distinguished. In accordance to previous publications there can be described, at least, 9 flow regimes, depending on the volumetric spatial concentration (C_{vs}) and the volumetric transport (delivered) concentration (C_{vt}): (1) Fixed bed without suspension, constant C_{vs}; (2) Fixed bed with suspension, constant $C_{vs;}$ (3) Sliding bed with suspension, constant $C_{vs;}$ (4) Sliding bed with suspension, constant C_{vt}; (5) Heterogeneous transport, $C_{vt} \approx C_{vs}$; (6) (Pseudo) homogeneous transport, $C_{vt} \approx C_{vs}$; (7) Homogeneous transport, $C_{vt} \approx C_{vs}$; (8) Sliding bed, sheet flow and (9) Fixed bed with suspension, constant C_{vt} (Ramsdell & Miedema, 2007) as seen in Figure 1.4.

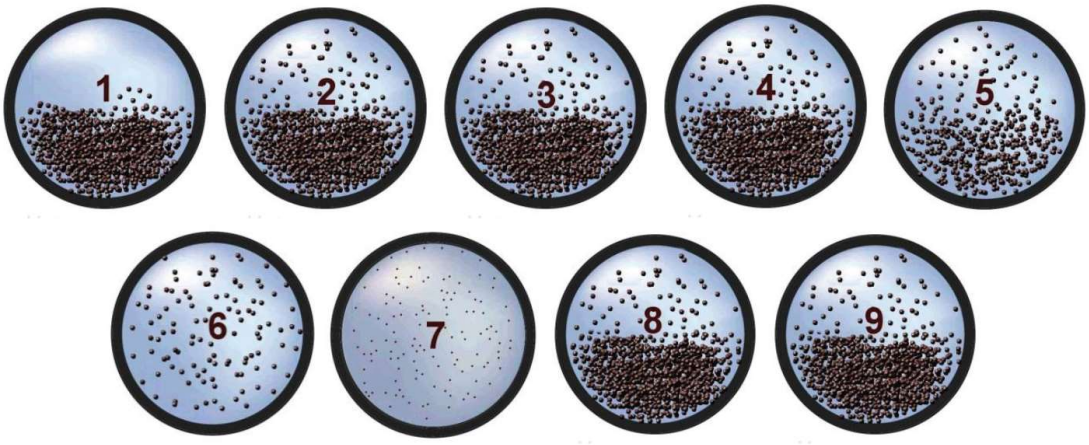

Figure 1.4 Pipeline carrying solid particles flows. Source: (Ramsdell & Miedema, 2007).

To know the flow pattern in a pipeline is important for the further design and prediction of operational parameters. Some of this parameters are those which will provide information related to the safety and the economics, for example:

- The mean mixture velocity ad its important values.
- The production of solids
- The frictional head loss
- The specific energy consumption.

In the case of this work, the two first points are the ones taken into account. The mean velocity of a pipeline is a simple parameter which characterizes the pipeline flow. It is defined as the bulk velocity, v, of a matter (liquid, solid or the mixture) and it is obtained from the volumetric flow rate, Q, so, from the mass balance equation it can be deduced that the expression for the velocity is,

$$v = Q/A \quad \textbf{(3)}$$

where A is the cross-section area of the pipe.

Related with this velocity it is important to define two main values: the deposition-limit velocity which is the threshold velocity at the initiation of the turbulent suspension and the minimum velocity at which the least energy is dissipated in slurry flow.

Describing this flow pattern it is also important to distinguish between the spatial volumetric concentration (C_{vi} or C_{vs}) and the volumetric delivered or transported concentration (C_{vt} or C_{vd}). The spatial volumetric concentration is described as the volume of solids divided by the volume of the mixture containing these solids, while the delivered concentration is based on a volume rate ratio:

$$C_{vd} = \frac{\dot{v_s}}{\dot{v_m}} = \frac{Q_s}{Q_m} = \frac{v_s A_s}{v_m A_p} = \frac{v_s C_{vs} A_P}{v_m A_p} = C_{vs} \cdot \frac{v_s}{v_m} \quad \textbf{(4)}$$

The volumetric spatial concentration is based on the volume ratio solids/mixture according to:

$$C_{vi} = \frac{v_s}{v_m} \quad \textbf{(5)}$$

In this work the spatial concentration will be obtained from the integration of the vertical concentration profiles while the delivered concentration is a given parameter.

1.3 ERT technique

Electrical Resistance Tomography (ERT) and other familiar techniques, such as EIT and ECT (Electrical Impedance Tomography and Electrical Capacitance Tomography), are nowadays used in the study of different fields and phenomena. The ability to watch what happens inside an optically inaccessible object provides immense advantages in numerous areas, from medical diagnosis to analysis and control of industrial reactors or detecting leaks in underground pipes (Sharifi & Brent, 2013).

ERT consists in the implementation of a current-pulse data capture system. It is composed by a sensor system, a Data Acquisition System and a PC with control and data processing software (Figure 1.5). The sensor system consists in pairs of electrodes equally spaced around the region of interest, usually in the form of a ring. Commonly, the configuration is of 16 electrodes per ring. Multiplane rings allow the possibility to obtain a three dimensional view of the process. The Data Acquisition System (DAS) is the component of the instrumentation that injects current and collects the quantitative information regarding the conductivity distribution inside the vessel. This component is connected to the electrodes and the PC containing the image reconstruction algorithms.

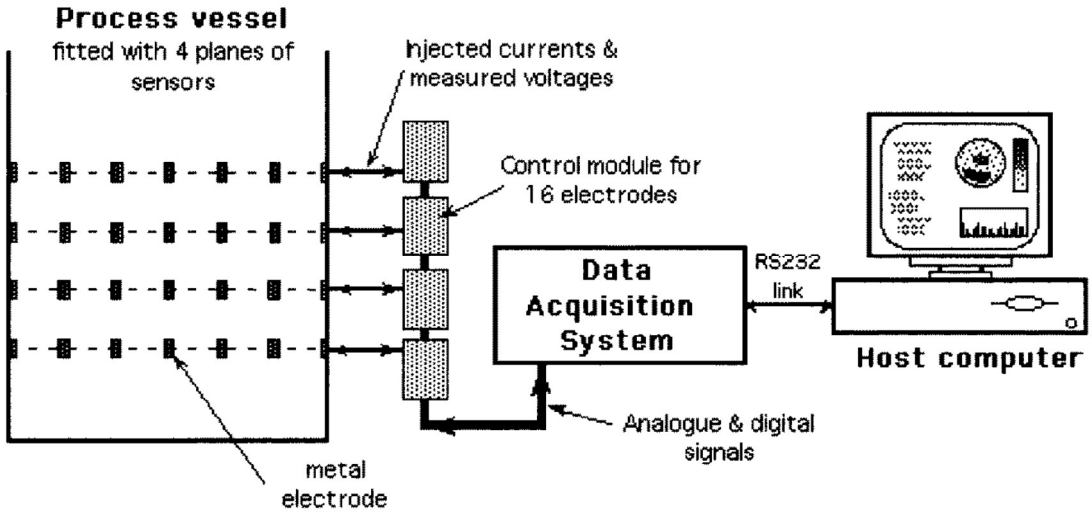

Figure 1.5 Structure of a typical tomography system. Source: (Dickin & Wang, 1996)

The main advantages of ERT with respect to other successful imaging modalities are its low cost, high speed and simplicity of usage compared to other techniques, e.g. Magnetic Resonance Imaging and Positron Emission Tomography. Furthermore, it also guarantees the safety of the experimenter and of the sensitivity of the object unlike methods based in radiation, for example, X-rays.

This kind of electrical resistivity techniques gained popularity between geophysicist during the 1920s. Those, used to insert arrays of metallic electrodes in the ground and inject current to map the sub-surface strata. One of the most

famous techniques in the geophysical world related with electrical resistivity is the cross bore hole, in which vertical poles containing annular electrodes are inserted into bore holes various hundreds of meters deep. In the 1970s, the ERT system as we know it nowadays (circular arrays of electrodes) was mostly developed in the Biomedical Engineering, where this technique was seen as an alternative to X-ray because of its handiness and low expenses, but its popularity has undergone for some limitations in this field. Most of the publications related with ERT application of the last years are related to the Geotechnical and Chemical engineering further than Biomedical Engineering, where EIT is usually applied. Today, ERT techniques are applied in the industry in pipes and piping systems in order to obtain multidimensional information of the features and conditions of the flow (Figure 1.6). Being able to obtain inside information of the opaque vessels has major benefits in the design, monitoring and control processes including vertical, horizontal and inclined pipes among others. Storage and mixing vessels are another application of the ERT technique, seen in many different kinds of industries. ERT is also used in the study of fluidized bed reactors. The different purposes of its application can be flow analysis, mixing analysis and phase distribution analysis.

Figure 1.6 Tomography applied in a slurry pipeline. Source: (Itoms).

In this work, ERT is used mainly for its outgiving usage and economic reasons explained before, to obtain maps of the distribution of solid particles in the flowing liquid in three cross sections of the pipe where tests are carried out.

1.4 EIDORS solver

Resistivity images are reconstructed by Electrical Impedance Tomography and Diffuse Optical Reconstruction Software (EIDORS). The goal of EIDORS is to provide a freely distributable and modifiable software for the reconstruction of electrical or diffusive optical data images (Adler & Lionheart, 2006). EIDORS software is developed in Matlab. The software includes solving the forward problem (simulation) and, on the other hand, reconstruction and the display of the images, called inverse problem. In this work, the focus is set on to the inverse problem: the reconstruction of the images. This inverse problem corresponds to a high speed reconstruction algorithm which, as said, is developed in Matlab to reconstruct the resistivity distribution.

ERT and EIT image reconstruction consist in a non-linear ill posed inverse problem. Ill-posed problems are those problems that do not fulfil the terms defined by Hadamard (1865-1963) for well-posed problems. He described that, for a mathematical model of physical phenomena to be well-posed, it is necessary to have these properties:

1. The solution exists,
2. The solution is unique,
3. The solution behaviour changes continuously with the initial conditions.

Thus, for an ill-posed problem such as the image reconstruction it is difficult to obtain stable and reliable results.

To solve the inverse problem, EIDORS uses an approach in which it is minimized the functional

$$\psi(\rho) = \|U - U(\rho)\|^2 + \alpha^2 \|L(\rho - \rho^*)\|^2 \quad \textbf{(6)}$$

with respect to the resistivity ρ. Where U is the vector of measured voltages and $U(\rho)$ the corresponding computed voltages. L is a regularization matrix, α is a regularization parameter and ρ^* is an a priori guess for the before mentioned resistivity, ρ (Vauhkonen, Lionheart, Heikkinen, Vauhkonen, & Kaipio, 2001). The solution is pursued iteratively by

$$\rho_{i+1} = \rho_i + \delta\rho_i \quad \textbf{(7)}$$

where the derivative $\delta\rho_i$ is solved from the following equation:

$$(J_i^T J_i + \alpha^2 L^T L)\delta\rho_i = J_i^T\big(U - U(\rho_i)\big) - \alpha^2 L^T L(\rho_i - \rho^*) \quad \textbf{(8)}$$

EIDORS solves this numerical problem by finding the zero root of the function with non-linear solver. For this work, in order to find the numerical solution for this problem, Gauss-Newton method is used.

Chapter 2. Objectives

The general goal to be reached in this work is to improve an imaging tool which will provide data for the better comprehension of the behaviour of non-Newtonian fluid carrying solid particles inside a pipe, which is supposed to lead in the future to further development advancement in the usage of slurry pipes. Specifically, this improvements are focused on the use of Electrical Resistivity Tomography technique as new imaging technique. For this reason, the focus of this thesis is to set in the development and adjustment of a computational tool which can read and represent the tomographic files and then, obtain values determining the concentration and distribution of particles in the flow to later relate it with other characterization parameters of the flow. Henceforth, it is centred in the adequate parametrization of the numerical problem and the further development of specific tools which provide the values describing the before mentioned characteristics of the two-phase flow. For this reason, smaller goals can be defined and checked in this work. This smaller goals are presented in the next paragraphs.

The first one of the objectives is to create, optimize and update the scripts used in the developing tool for the images post-processing. This is made with the use of an open-source code called EIDORS. As explained, EIDORS uses scripts defined in Matlab. Also the post-processing tool of the images and data analysis is developed in Matlab.

The second goal is to set an appropriate visualization of the tomographic files. Since this visualization is a numerical solution of an ill-posed problem, check the value of the main parameters used in EIDORS to interpret the images has also become part of this work. On this account, sensitivity analysis for specific parameters, such as the hyperparameter and the background conductivity, are done also in this work in order to see and determine the range of influence of each one of these parameters and set them to an appropriate value in order to obtain the most representative 2D images.

The second objective is to analyse, discuss and set the adequate criteria in all the procedure and methods related with the calculation of the characterisation values of the flow. It is discussed the appropriate usage of the calibration files in order to obtain the correct elements concentration values which will determine the success in the results obtained.

Finally, it is important to link the results obtained by the scripts, 2D tomograms, 1D concentration profiles and in situ measured average concentration with other properties and images of the same tests obtained with other techniques, different than the ERT, describing the flow such as the velocity, and giving them the appropriate interpretation in order to understand the behaviour of the two-phase flow.

Chapter 3. Materials and methods

This chapter includes a description of the physical materials and tools used in the Water Engineering Laboratory of the Czech Technical University in order to perform the tests as well as the methods used in the computational model tool used to process the Electrical Impedance Tomography files obtained from the physical model, including a description of the most relevant parameters: the hyperparameter and the background conductivity.

3.1 Laboratory test instrumentation

The Electrical Resistivity Tomography physical tool used to carry out the tests described in this work is a University of Cape Town design which has been shared with the Czech Technical University. It consists in a 3 rings of electrodes stepped around the cross-section of the pipe where a current source and sink are applied to adjacent pairs of electrodes and the resultant peripheral voltages, determined at the same time by 16 differential amplifiers hardwired to adjacent electrode pairs, are recorded. A single layer (ring with 16 pairs of electrodes) is shown in Figure 3.1.

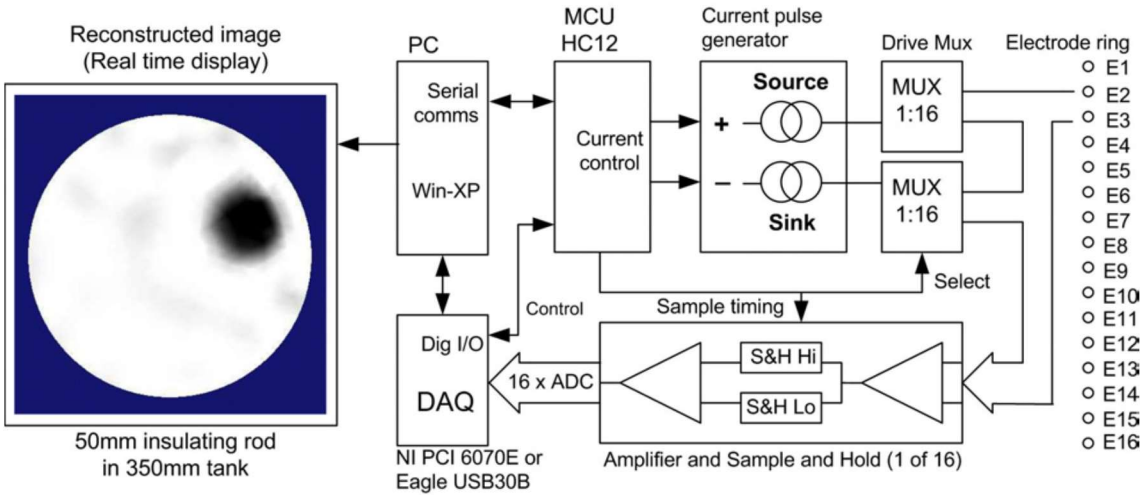

Figure 3.1 Basic current pulse ERT system for single ring of 16 electrodes. Source: (Wilkinson, Randall, Long, & Collins, 2006).

In this single layer it can be appreciated the following sections of the instrument: first the current source and sink circuits, which must be accurately balanced, next the current drive multiplexers (2x16 way) which select the current drive electrode pair, then the 16-channel amplifier with sample and holds which simultaneously measures the differential voltages between adjacent measuring electrodes and finally the processor which controls the current pulse and measurement timing and the multiplexer (Wilkinson, Randall, Long, & Collins, 2006).

This whole system for the ERT is controlled by a personal computer that is used for data capture and real-time visualization. The software for this computer is written in C++.

As mentioned, for the laboratory experiments carried out in this work 3 rings have been implemented in the vessel to obtain 3 different sections of it at each time step. This rings are located in the laboratory equipment. This equipment consists in a pipe loop located in the water Engineering Laboratory of the Czech Technical University in Prague. This loop is composed of pieces of a polyethylene pipe (with an interior diameter of 51.4 mm), blank pipe in Figure 3.2, and a piece of transparent acrylic pipe (with an interior diameter of 50.0 mm), grey pipe in Figure 3.2. The total length of the loop is 22.96 m and its volume is 45.08 l. The length of the horizontal section is 6.20 m. The mixture is pumped with an EBARA 3M 40-200/7,5 kW pump which is driven by an electric motor with a variable frequency converter TECO GD100-011G-4 11 kW. Pump parameters are: power 7,5 kW, impeller diameter 200 mm, maximum flow 11.67 l/s, total head from 58 m to 44m (valid for water for maximum flow) (Peník, Kesely, & Matoušek, 2016).

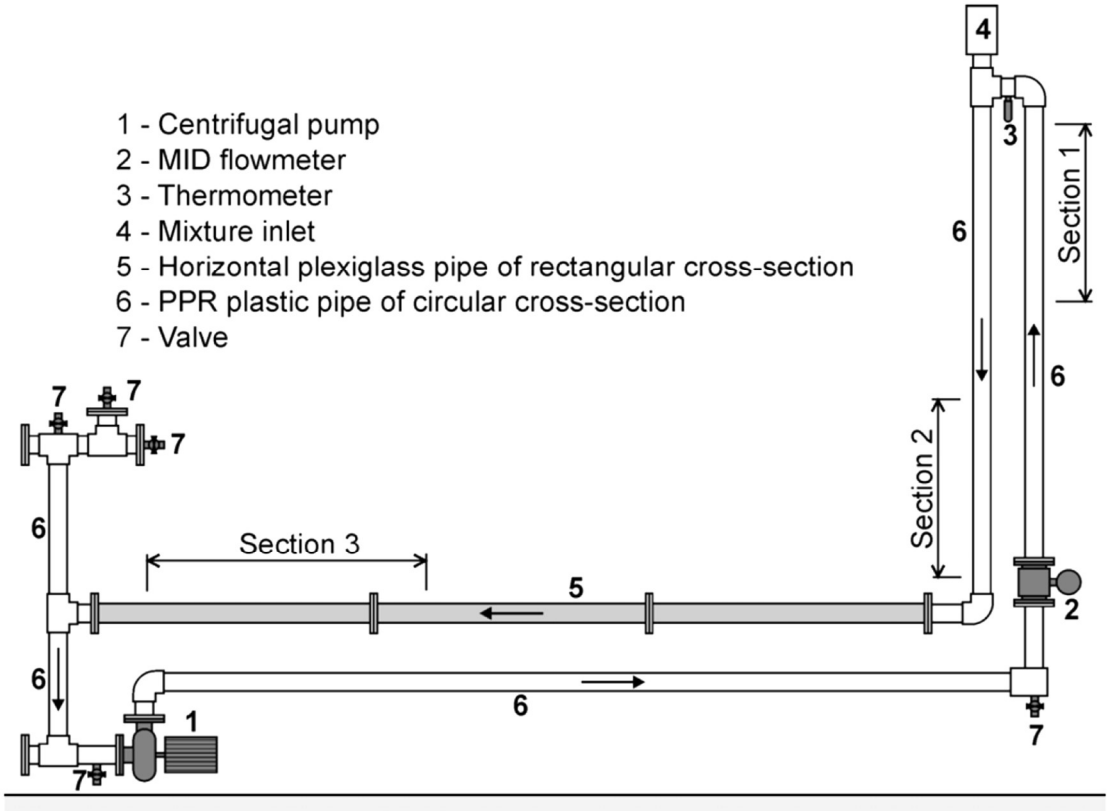

Figure 3.2 Test pipe loop in Water Engineering Laboratory of the Czech Technical University (Prague). Source: (Peník, Kesely, & Matoušek, 2016).

Tests are carried out with a mixture composed by Carbopol as the carrying non-Newtonian liquid and glass coarse particles as transported solid.

Carbopol powder is a carbomer[1] water soluble vinyl polymer, used as stabilizing, suspending, thickening and gelling agents in many industries. It consists in an acidic powder of particle from 2 to 7 microns which, once is dispersed in water and after neutralization process, forms a non-Newtonian solution of the kind Herschel-Bulkley[2] (thickened tailings kind). The values of its rheological parameters depend on the concentration of the powder that is mix with the water. The main reasoning for using Carbopol in the experiments done is that it is a transparent fluid so observation of the behaviour of the coarse particles mixed in is possible and also that different concentrations, therefore, properties can be obtained without difficulty.

The coarse glass bed particles used in all of the tests done correspond to the type TK1.5 with a median diameter, d_{50}, of 1.5 mm. The sieving test done, showed that all grains were finer than 1.61 mm and all grains were coarser than 1.49 mm. Its density is 2488 kg/m^3.

[1] In organic chemistry, a carbomer is an expanded molecule obtained by insertion of C_2 units into a given molecule.
[2] Explained in section *Non-Newtonian fluids*, in the first chapter (Chapter 1. State of art).

3.2 Computational model

ERT measurements acquired with the physical instrumentation are processed by EIDORS as a finite element method mesh and images are obtained from the solution of the numerical problem stated in the first chapter of this dissertation.

Accordingly, the resulting images can be understood as the values of the elements in a matrix with dimensions of 256x256. This matrix values can be plotted by Matlab as a contour image in order to give an easier, non-numerical, interpretation of the results.

In order to calculate the concentrations, for each test, two first tomographic files are processed to calibrate the model. The first one contains a calibration image with only static Carbopol (clear Carbopol) so that null concentration is correctly achieved. The second one, contains a mixture of Carbopol and particles without movement (null velocity gradient) so that the particles are completely settled in a bed at the ground of the pipe and, consequently, the maximum possible concentration is reached. So, the concentration is obtained by setting the maximum value of the concentration to the maximum value obtained from the mentioned fixed bed calibration ERT file and the minimum concentration value is, at the same time, assigned to the minimum value in the clear Carbopol calibration file.

The maximum concentration value is considered to be, by previous literature, of around the 60% and the lowest value of the concentration is considered to be the 0%. Once this both values are related to the maximum and minim values obtained with both calibration files, it is only necessary to interpolate between them to find the rest of the values of the test measurements matrixes. Accordingly, the concentration mapping consists also in a 256x256 elements matrix with values theoretically between the range of 0 and 0.6.

Once this 2D map of concentrations is obtained for each of the files, a chord average is calculated along the vertical axis to obtain a 1D profile and from its integration also an average concentration for the whole cross-section is obtained and related with velocities in the pipe.

3.2.1 Scripts developed

The structure of the computational model, in order to perform all the results, is shown in the following graphic (Figure 3.3). This graphic shows the main scripts and phases concerning the computational model used in this thesis.

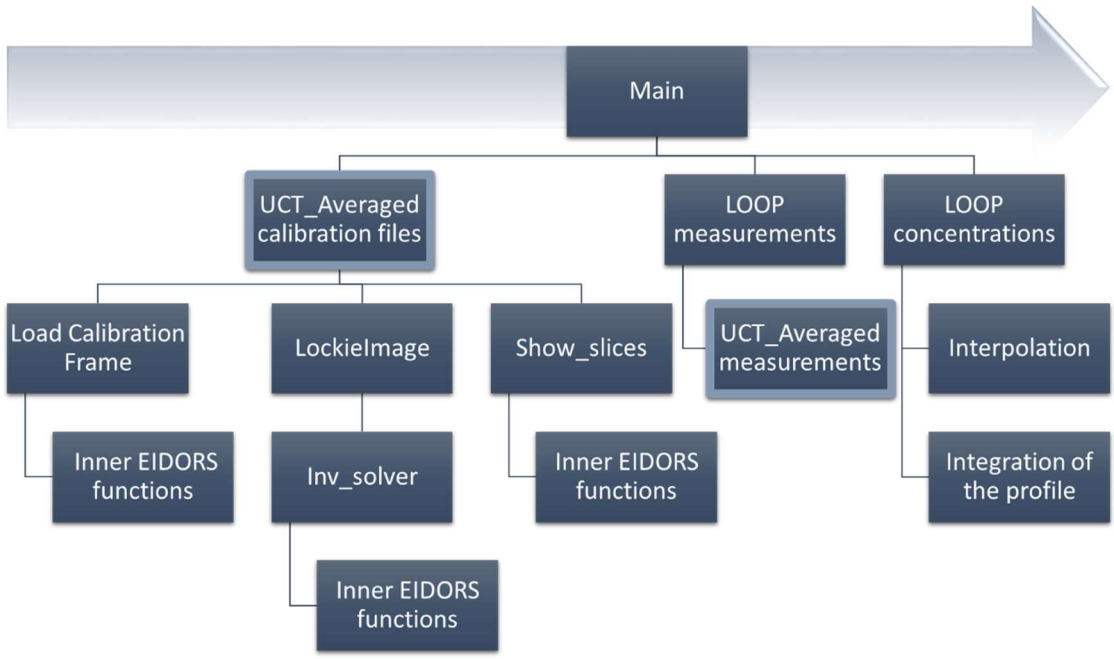

Figure 3.3 Sketch of the program performance of the scripts.

From the main menu of the scripts the function *UCTImage_Averaged* is called in order to obtain the images for the files, both in the calibration and in the measurements. This function is the main script to obtain the before mentioned value matrixes for the images, which will later be plotted as a contour figure in the main script. *UCTImage_averaged* is based on *UCT_LoadDataFrame*[3], but it includes some modifications of the code.

Inside this function another script is called to open the .*cal* files (calibration files set for EIDORS parameters for all the measurements). This new script is called *LoadCalibrationFrame*. This function extracts the current and no current data from the calibration set. Current data is data collected when current is applied to the container, in this case the pipe, while no current data is data obtained when no current is applied in the same tank when there is an homogeneous solution. This script was developed by the UCT and same function can be found with the name *UCT_calibration_file*[4].

[3] Can be obtained from EIDORS website.
[4] Can be obtained from EIDORS website.

Later, *UCTImage_Averaged* calls the function *LockieImage*. This function was originally a modification of *moving_tank_objs*[5]. In this modification, it offers solely the possibility of the inverse model case selection for the image reconstruction. One of the main updates done in this work is the introduction of the user definition of some of the methods and parameters for the inverse calculation in this script instead of using the default ones set by EIDORS. After the selection of the case and the parameters values it calls the inverse calculation. For this thesis it is developed the case 1, where all the following parameters and solving methods are chosen as a structure of the inverse model selected, *imdl*:

- imdl= mk_common_model('c2c',16);
- imdl.RtR_prior= 'prior_laplace';
- imdl.solve='inv_solve_diff_GN_one_step';
- imdl.jacobian_bkgnd.value=bk;
- imdl.hyperparameter = rmfield(imdl.hyperparameter,'value');
- imdl.hyperparameter.func = @choose_noise_figure;
- imdl.hyperparameter.noise_figure= NF;
- imdl.hyperparameter.tgt_elems= 450:454;
- imdl.hyperparameter.xyzr_targets=[256; 256; 1; 0];

For instance, *mk_common_model* is a function used in EIDORS in order to select common EIT (Electrical Impedance Tomography, used similarly as for ERT) FEM models, so that users do not need to re-write common code. The option selected in this work, '*c2c',16'*, represents a 2D circular model with 576 elements.

The *RtR_prior* defines the method used to calculate the regularisation matrix. In this case the '*prior_Laplace*' option is used. This is based in the regularization method graph-Laplacian. A graph Laplacian regularizer assumes that the original image (patch) is *smooth* with respect to a defined graph (Pang & Cheung, 2017).

And the iteration solution is calculated by means of the Gauss-Newton method solver algorithm *'inv_solve_diff_GN_one_step*' using the approach of Adler & Guardo in 1996 (Adler & Guardo, 1996). The Gauss-Newton method is a highly efficient iterative method used to solve nonlinear least- squares problems. This can be seen as a modification of the Newton method to find the minimum value of a function.

Finally, some of the most significant parameters are also designated. One of the main modifications in the code is that, is that most significant parameters such as the hyperparameter Noise Figure selection and the background conductivity, are now defined by the user with the variables *bk* and *NF*, and this definition can be

[5] Can be obtained from EIDORS website.

done from the main script so that a user without further knowledge in EIDORS can automatically set them without going deeper into the scripts.

After all the computational EIDORS model description, *Lockiemages* calls the inverse solver with the function *inv_solve*. This gives back vector values for each of the planes read in the tomographic file which are later reconstructed as an image with a modification of the EIDORS function *show_slices*.

The script *show_slices* , usually is used as a visualization tool in its original script done by EIDORS developers but, for this case, the out image call is supressed and it is only used to obtain the matrix of 256x256 values for the image as a reconstruction of the vectors obtained in *show_slices*.

This *UCTImage_Averaged* process is repeated for all the calibration files and the measurements.

Once all measurements have gone through this scripts they are split into ring matrixes of 128x128. The fourth matrix obtained in this splitting process is empty as it does not contain any ring (there are only 3 rings in the pipe and, thus, it is discarded.

Then for each one of the points in the ring the interpolation to concentrations is done, and after the chord-average on every row gives the 1D profile of concentrations which by integration also gives the average concentration of an specific cross-section (ring of electrodes) at each measurement.

Later in the program, this values will be related with the delivered concentration and the velocity, obtained with other measurement tools, in the plotting graphs in the main menu.

3.2.2 Parameters

As explained before, in order to reconstruct the images in an appropriate way, some parameters have to be set in advance in the function *LockieImage*. A great part of this work includes the adequate objectively setting of this parameters to obtain the desired results in a standard way, avoiding human selection (heuristic methods).

Some of these parameters regarding the computational model are explained in order to understand the posterior results achieved and their discussion. Thereupon, in this section there are introduced two parameters related with the computational solver which have been objective of this work: the hyperparameter and the background conductivity.

a. Hyperparameter selection: Fixed Noise Figure

As said, the processing of the ERT images is an ill-conditioned problem in which regularization is used to calculate a steady and accurate solution, by incorporating some sort of prior knowledge into the solution. The hyperparameter is used to control the balance between conformance to data and conformance to the prior (Graham & Adler, 2006).

The image reconstruction problem is essentially undetermined and characterized by a system matrix with large condition number. By imposing some other conditions (priors), such as the image smoothness, some of the instability and noise dominance problems can be overcome. The balance between solution conformance to the measured data and conformance to the prior is controlled by a scalar called hyperparameter labelled λ.

Similarly to the expression in (6) it can be written equation (9). Considering $x = (\sigma_2 - \sigma_1)/\sigma_1$ a change in a finite element conductivity due to a proportional change in difference signal $z = (v_2 - v_1)/v_1$ over a time interval (t_1, t_2). Since σ_1 is an unknown, x is interpreted as the proportional change in conductivity with respect to the unknown initial conductivity, $x = \Delta\sigma/\sigma_0$. If small changes around the background are considered the x and z can be linearized as

$$z = Hx + n \tag{9}$$

where H is the sensitivity matrix and n is the measurement noise system. Each element of H can be computed as $H_{ij} = \left.\frac{\delta z_i}{\delta x_j}\right|_{\sigma_0}$ and relates a small change in the i^{th} proportional difference measurement to a small change in the proportional conductivity j^{th} element. Thus, H is a function of the finite element mesh, the current injection pattern, and the background conductivity, σ_0. This background conductivity is usually considered as homogeneous.

Then, in order to overcome the ill-conditioning of H it is used the following expression, similar to equation (8),

$$\hat{x} = (H^T W H + \lambda R)^{-1} H^T W z = Bz \quad \textbf{(10)}$$

where $\hat{x}$ is an approximate of the true proportionate change in conductivity distribution, R is a regularization matrix, λ is scalar hyperparameter that rules the regularisation amount and W manners the system noise.

It is difficult to develop and validate methods of objectively selecting the hyperparameter. Some of the methods known for the selection of the hyperparameter, among others, are:

1. Heuristic selections
2. Generalized Cross-Validation
3. L-Curve approaches
4. *BestRes*
5. Fixed NF Results

In this work, and based in previous studies analysis, the method chosen for the selection of the hyperparameter is the fixed NF. The main advantage of using an objective method to select the hyperparameter is that the range of possibilities for the values set in the Noise Figure is much more bounded than the options for the hyperparameter which can have several different orders of magnitude.

NF stands for Noise Figure and represents a ratio of signal to noise ratio (SNR) in the measurements to SNR in the image.

$$NF = \frac{SNR_{in}}{SNR_{out}} = \left(\frac{mean[z_c]}{\sqrt{var[n]}}\right) / \left(\frac{mean[Bz_c]}{\sqrt{var[Bn]}}\right) \quad \textbf{(11)}$$

The signal used in this definition is $z_c = Hx_c$, where x_c is a small contrast in the medium centre (targeted element). This script is already created in EIDORS and the user selects an NF value and the corresponding λ is found by means of the bisection method search technique.

Experience has shown that figures in the range 0.5 to 2 consistently lead to good reconstructions while, the associated λ value associated can range over several orders of magnitude depending on the configuration (Graham & Adler, 2006). In the conclusion of their work, Graham & Adler, point out that Fixed NF method is “repeatable and, in applications with realistic noise levels, will produce consistent stable reconstructions that are as good as heuristic selection”. The choice of a

hyperparameter selection method permits the final user to perform the image reconstruction without the need of having to manually adjust the hyperparameter.

For the automatic hyperparameter calculation it is also important to set the target elements. This target elements are the indices of the finite elements which will be used to simulate a small conductivity change in order to calculate the noise figure

b. Background conductivity

The conductivity of an element is a measure of its ability to conduct electricity. The unit in the SI for the conductivity is Siemens per meter (S/m). Deionized water has a conductivity of about 5.5 µS/m at 25 °C while typical drinking water in the range of 5–50 mS/m and sea water about 5 S/m.

The background conductivity can be physically determined by setting two electrodes separated by a fixed distance (such as the electrodes that are placed in the system). In EIT and ERT the main goal is to detect a compact conductivity variance and classify it as an increase or decrease in conductivity with respect to the background one. At each step, the Jacobian is calculated, the linearized problem is solved, and the guess conductivity distribution σ_0 is updated adding the calculated contribution $\Delta\sigma$. Generally, the algorithm stops when the relative variation of the residual between consecutive iterations drops below a threshold or a user-defined maximum number of iterations is reached (Samorè, Guermandi, Placati, & Guerrieri, 2017).

Usually, in the image reconstruction an homogeneous background is supposed, and, sometimes, this assumption can introduce a mismatch between the reference measurement and the linearization point (Grychtol & Adler, 2013).

The value at which is adjusted the background conductivity scales the value of the contrast between points. Properly scale this contrast for all images obtained in the same test, so that all values between different measurements can be correlated, is also an important issue to make the images to be reconstructed more reliable.

To summarize, background conductivity defines the scale of the values obtained in the post-processing, so it is important to fix in all the files their real background conductivity value so that they can be related between them with proportionality.

Chapter 4. Results and Discussion

In order to attempt and verify the effectiveness of the improvements and changes in the program, six different tests with Carbopol have been carried out in the laboratory and its images have been processed by the scripts developed. This tests are presented in Table 4.1. For each test there is a different measurement of the background conductivity and a different number of captures for each one of the scripts (measurements). These are also presented in the same table.

Since Carbopol is a very unstable fluid and rheological changes are considered to happen during the development of these tests, also an extra test done with water has been executed by the scripts to ratify the performance of the computational tool designed, since water characteristics are more stable.

#	Test ID number	Number of measurements	Background conductivity
1	CBP0,130a_TK1,5_20140729_a	16	[0.649-0.677]
2	CBP0,130a_TK1,5_20140729_b	16	[0.677-0.647]
3	CBP0,140a_TK1,5_20140716_a	12	[0.600[6]-0.683]
4	CBP0,140a_TK1,5_20140723_a	18	[0.700-0.670]
5	CBP0,175b_TK1,5_20140803_a	18	[0.720-0.740]
6	CBP0,175b_TK1,5_20140803_b	17	[0.731-0.760]
	waterTK1,5_20140704_a	*11*	*0.378*

Table 4.1 Tests processed and analysed for this work.

For each test, it is possible to analyse the evolution of the three different rings set along the pipe for each one of the measurements carried out.

All the results have been gathered together in the Appendix I. For this memoir and discussion, instead, only few of the most representative ones will be shown, in order to give a complete but non-distracting comprehension and discussion for the reader.

[6] There was is no data of the value, so a guess value has been introduced.

4.1 Analysis of Carbopol-based slurry

4.1.1 Criteria selection

For the purpose of choosing the results to be the most truthful as possible some different criteria are discussed before the lasts criteria and the finale results presented.

a. Calibration

For instance, it can be demonstrated that depending on the calibration file used to calibrate the computational model the values obtained in the concentration may vary. Each one of the measurements has its own calibration file. For all of these calibration files the actual maximum concentration may not always be the 60%, especially when the concentration of particles in the calibration bed used is quite low. However, the maximum value obtained in the calibration file is always set up to the 60% (maximum concentration possible). This may bring a posterior error in the calculation. For so, it is contrasted the use of the own calibration bed file for each one of the tests carried out with the case where the same calibration file, with a very high concentration, is used as the calibration file for all the different tests of study. For this reason, all the files are processed with the different criteria and, the values obtained are compared, in order to decide which of the criterion is best fitting for the obtaining of the final results.

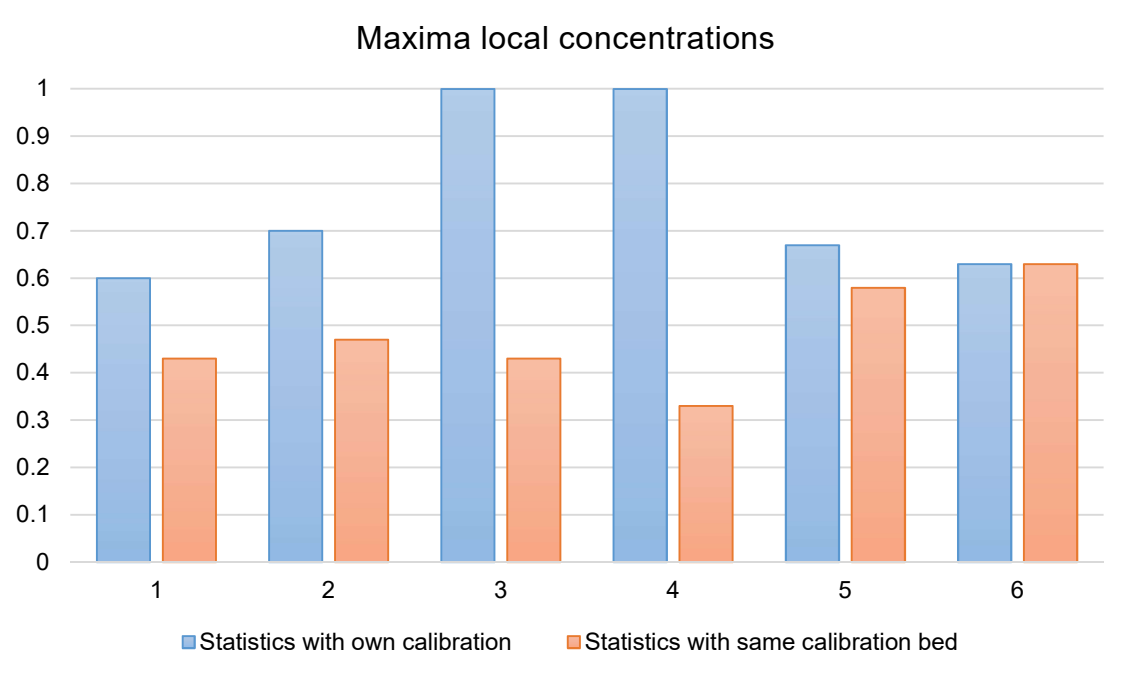

Figure 4.1 Comparison of maxima local concentrations obtained in the 1D profiles for all the tests (numeration following Table 4.1) between calibration beds.

In the comparison between the two possibilities for the calibration bed it is used the calibration bed file of CBP0,175b_TK1,5_20140803_b as the reference bed, since the images showed the higher values of concentration among all tests tried out. If the maximal local concentration obtained is observed it can be appreciated that, if the same concentration bed is used for all the tests, the maximum local concentration obtained for each one of the tests is lower than when their own calibration bed is used (Figure 4.1).

Besides, it can be appreciated in that the differences between the combined are not very abrupt in the tests CBP130s and CBP175s but have greater differences for the files CBP140s where exaggerated concentrations compare to the real ones are obtained while using a different bed shows the lower concentrations for all the tests. For this reason, this both files are considered key values in the decision of the final criteria used and are used with the video images obtained with other methodologies to compare and decide the final criteria to be used in the calculation for the definitive results.

Also, comparing the results obtained in the post-processing of the tomographic files it can be seen that for CBP0,140a_TK1,5_20140716_a, the values for the concentration are quite similar to the CBP0,130a_TK1,5_20140729_a, as the values obtained for both test with the same calibration bed in the case of local maxima are similar. Also, with the video images recorded for both test, it can be appreciated that both files show similar initial concentration and behaviour (Figure 4.2 and Figure 4.3).

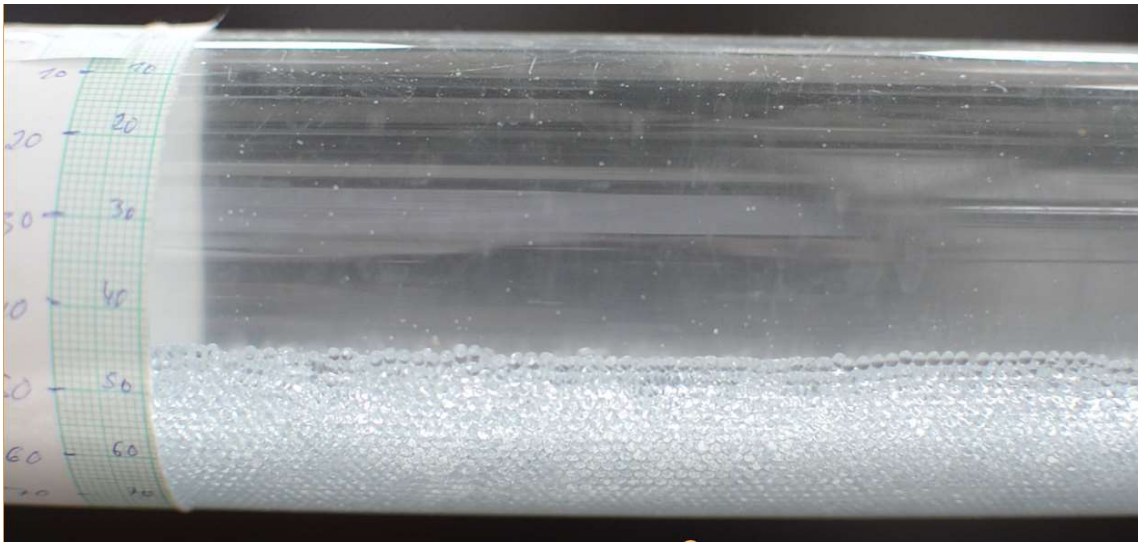

Figure 4.2 Test: CBP0,130a_TK1,5_20140729_a .Video image for measurement 1. The bed shows quasi-static behaviour.

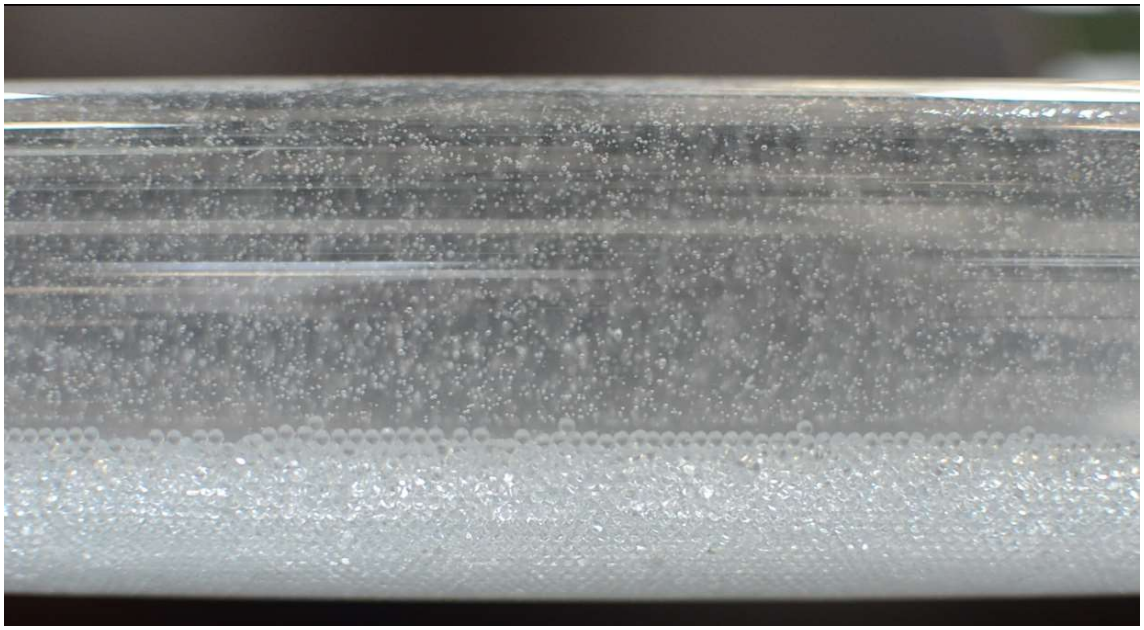

Figure 4.3 Test CBP0,140a_TK1,5_20140716_a. Video image for measurement 1. Bed shows completely static behaviour.

For this reason, the CBP0,130a_TK1,5_20140729_a calibration bed file is used for the post-processing of the file CBP0,140a_TK1,5_20140716_a in order to see if not using a unique bed but similar beds for similar tests could work out.

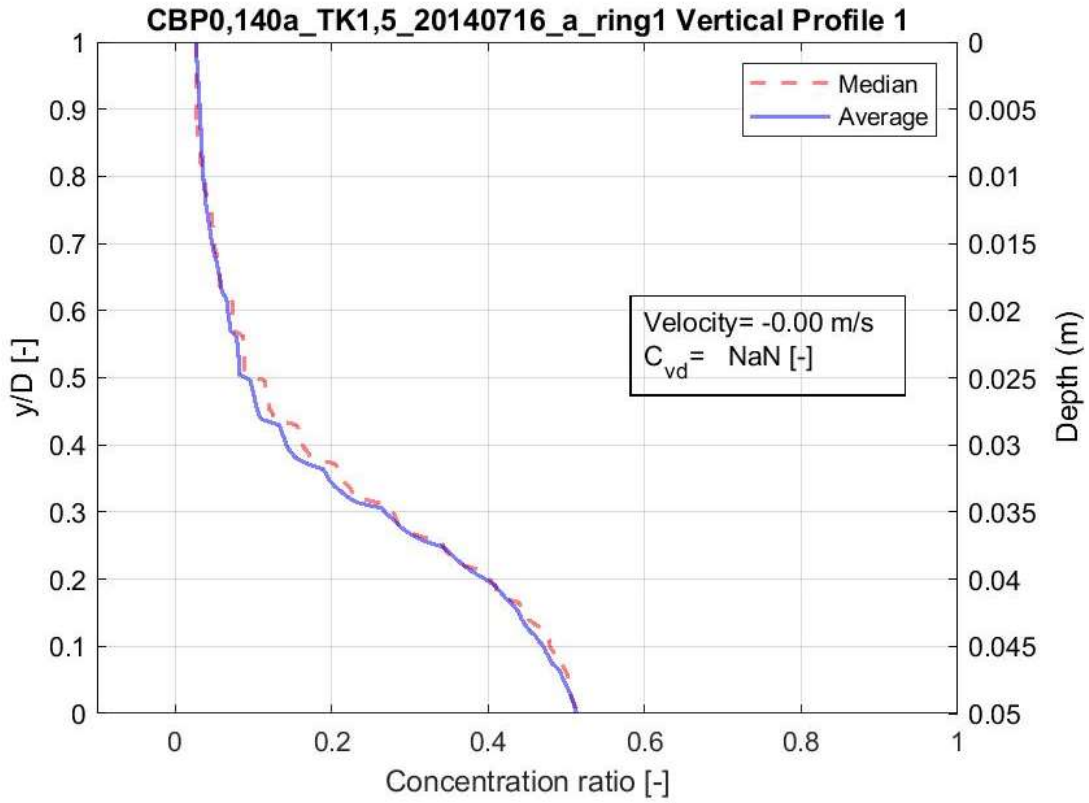

Figure 4.4 Test CBP0,140a_TK1,5_20140716_a-, ring 1, measurement 1. 1D Profile for concentration of particles.

Nevertheless, with the use of CBP0,130a_TK1,5_20140729_a bed as the calibration bed for the file CBP0,140a_TK1,5_20140716_a, the profiles obtained show a maxima of a 50% (Figure 4.4), and in comparison with the videos, it can be noticed that there is a steady packed bed where the concentration should be of the 60% (Figure 4.2 and Figure 4.3), so also this “similar test beds” use is discarded.

On the other hand, when using the common calibration bed, local maximum concentration for this files are too low.

In conclusion, for most of the test their own calibration files show better results than when using a common calibration file. Nonetheless, during this work, measurements during some of the test show lower or higher values than the ones stablished as the minimum and maximum in the calibration files, respectively. Moreover, the calculated concentration can even achieve negative values or higher values than the theoretical ones expected.

The values over the maximum can be explained by the assumption that the maximum value set with the calibration file used may not be really the maximum concentration possible, as particles might be not completely settled or the settling configuration may not be the denser, namely poor calibration.

For the case of the lowest concentration values, it is possible to interpret that, since increasing the velocity may also increase the energy losses by the turbulent flow, at the same time, this kinetic energy losses may be converted into heating energy and the temperature may raise and thus, changes in the rheological properties of the fluid may happen. So this change in the conductivity of the fluid can be interpreted as a new 0% concentration value.

For all this reasoning and after the analysis the developed program is modified. A recalibration for the maximum and minimum concentration is added during the running of the script. First of all, in this recalibration modification, there is a general check for the maximum concentrations. Since the measurements of the images are done before the interpolation of the concentrations, if in any measurement of the file has a higher value than the one set as the maximum concentration by the calibration file, this higher value is set as the 60% concentration before starting interpolating between concentrations. Then, in every one of the interpolations for each measurement of the test, it is checked whether there is a lower value than the actual value set for the 0% concentration. If so, this value is set as the new minimum concentration for further measurements.

For lower values of the concentration, the 0% concentration (clear Carbopol) is supposed to be a non-stationary value due to the rheological component, and as

a consequence, a recalibration is done at each time step of the calculation for the concentration checking if in the calculating measurement there is a lower value. By using this recalibration the results obtained look more realistic.

Once the recalibration is set the new maxima local concentration look like the figure below (Figure 4.5). It can be appreciated that results make more sense with the new recalibration and using their own calibration bed as usually for the lower velocity values a static bed can be appreciated and thus, concentration should be considered of around 60%.

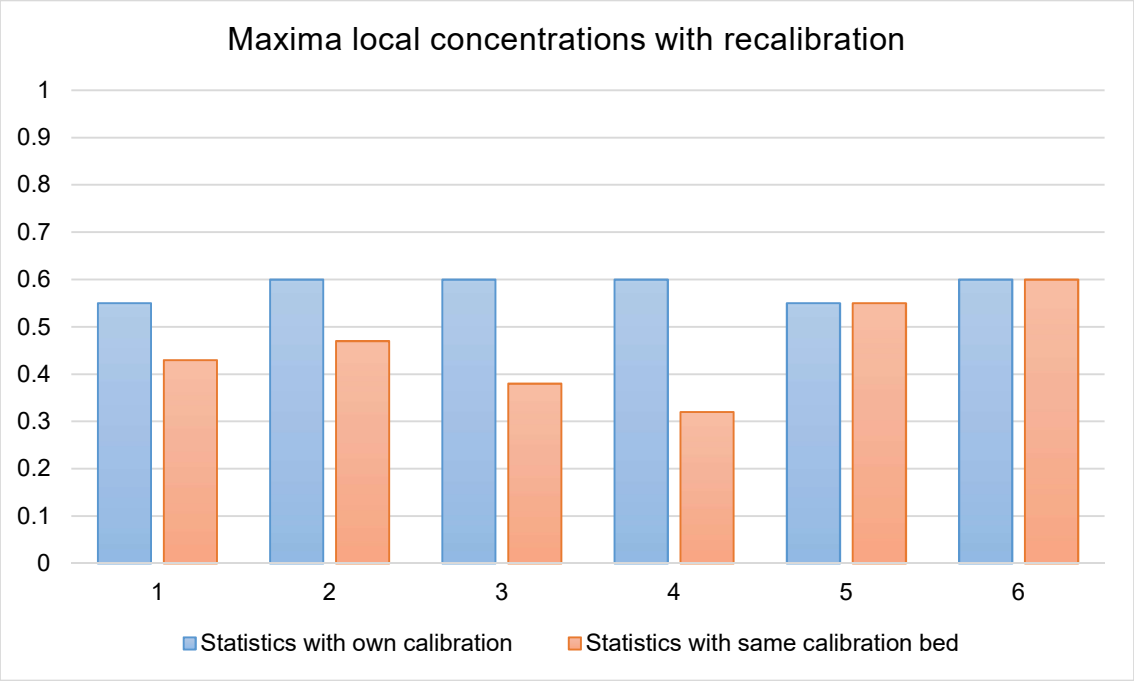

Figure 4.5 Comparison of maxima local concentrations obtained in the 1D profiles for all the tests (numeration following Table 4.1) between calibration beds with recalibration.

Also, once set this recalibration, it can also be seen that, for the maxima mean concentrations measured in the whole cross-section by integration of the 1D profiles by means of the trapezoidal integration, differences between the files become less noticeable when using the own calibration bed than when using the same calibration bed for all files (Figure 4.6). Usually, using the own bed for the calibration not only increases the maximum local value but all the values in the 1D profile curve Consequently, when integrating this values, usually the own calibration file criteria gets higher average concentrations, which look more realistic.

For all the tests, the minimum concentrations obtained have been lower than the theoretical ones expected. Differences between values for the same files for all the possible combinations are not remarkable, excepting for the case of CBP140 files where there is a jump between values when using their own calibration file or the common calibration.

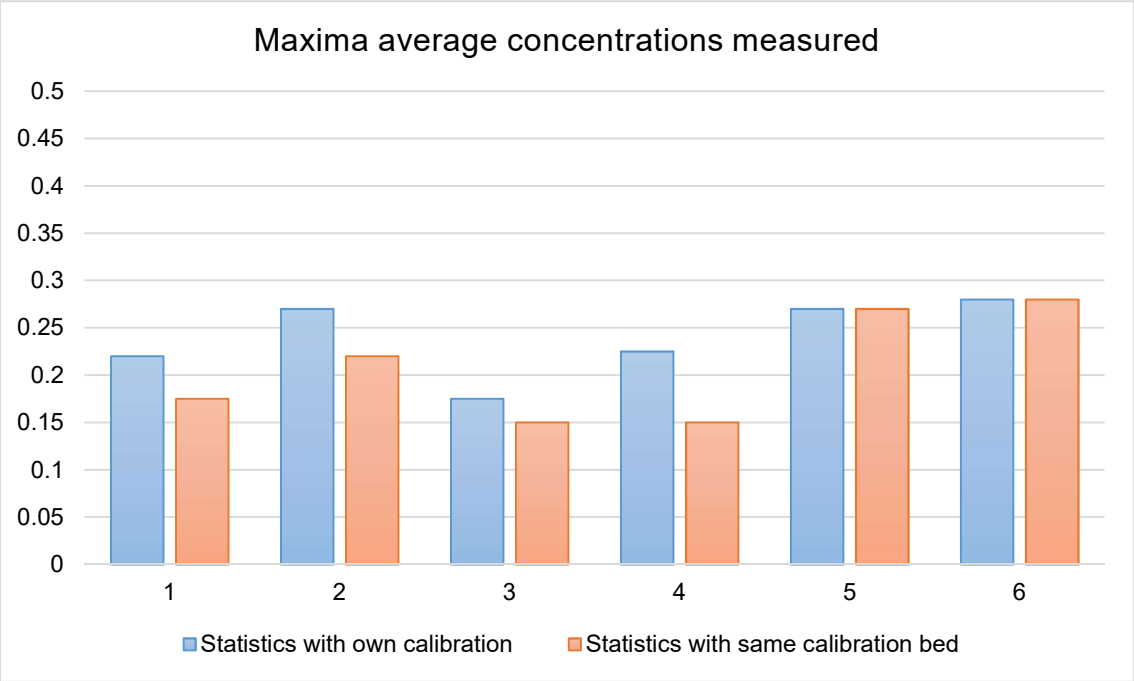

Figure 4.6 Comparison of maxima average concentrations (C_{vi}) obtained for all the tests (numeration following Table 4.1).

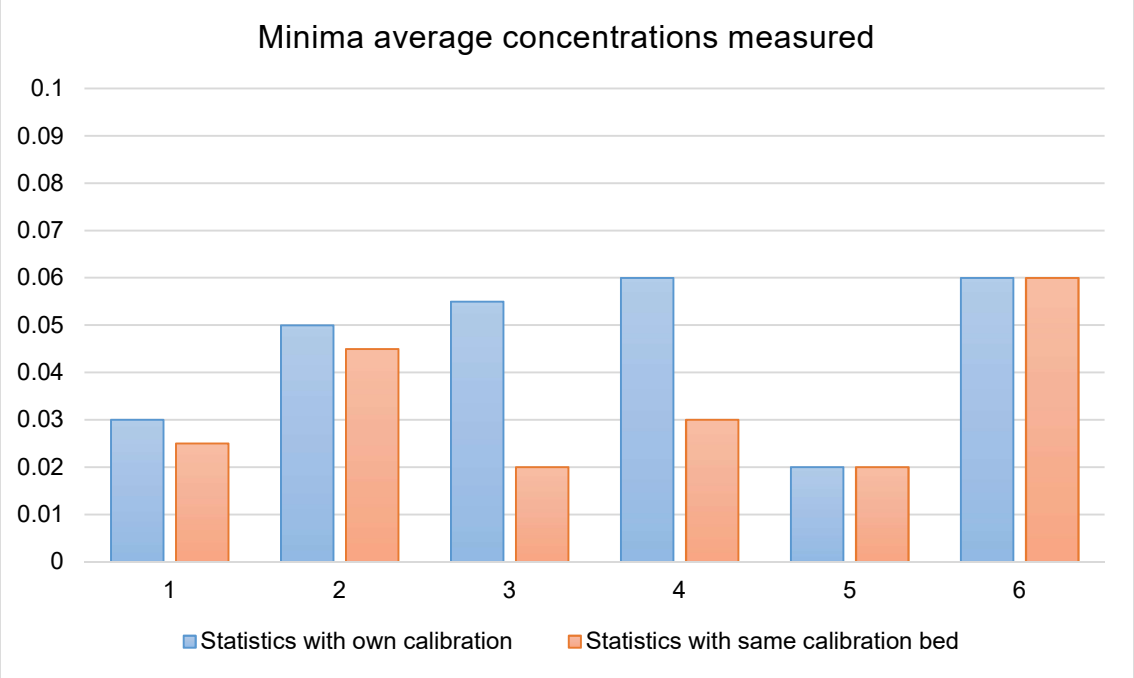

Figure 4.7 Comparison of minima average concentrations (C_{vi}) obtained for all the tests (numeration following Table 4.1).

To summarize, after the criteria analysis it is decided that results are presented using their own calibration bed plus an in time recalibration and trapezoidal method is used for the integration of the results, since this combination looks like the most fitting one.

b. Hyperparameter sensitivity analysis

As it has been explained in previous chapters the hyperparameter controls the smoothness of the image. This hyperparameter needs to be set in every one of the measurements obtained in order to achieve reliable images. Therefore, instead of setting in it manually Fixed Noise Figure method has been introduced in the code with the purpose of automatically achieving an adequate value of the hyperparameter for the visualization of the images. Nevertheless, the value for this Fixed Noise Figure is checked by means of a criteria analysis which is now presented.

Different values for the concentration are obtained from the ERT image by changing the Noise Figure value. As smaller the value of the noise is set, images tend to smooth the difference between neighbouring points (Figure 4.8). This changes on the definition of the image have an impact on the calculation of the concentration values, and different distribution profiles are obtained as seen in Figure 4.9.

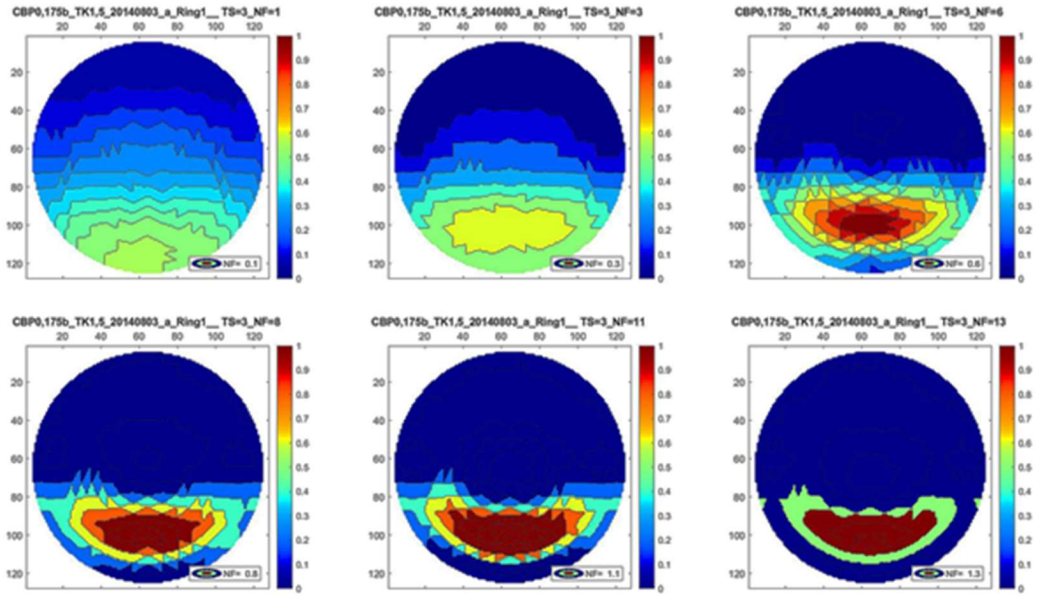

Figure 4.8 Test CBP0,175b_TK1,5_20140803_a. Some representative values obtained for the same measurement depending on the Noise Figure fixed.

Also, in this hyperparameter influence analysis it can be seen that values obtained near the wall of the pipe usually are lower even when there is a bed concentration. That may be because of the influence of the currents injected near the edges of the pipe by the electrodes, thus an instrumentation error and, if corrected, values may be better fitting.

Tests are completed by changing the NF value from 0.1 to 1.5. Usual working values for the Noise Figure range between 0.5 and 1 and provide optimal values for the selection of the hyperparameter (Graham & Adler, 2006), which can have a wider assortment of values (even orders of magnitude). In this work experiments, the most accurate images are obtained with values that usually range between 0.2 and 0.3.

In this case of study, for values above 0.5 the shape of the 1D profile presents a peak in the bottom bed which is not considered real, and subsequently this higher values are discarded in the use of the reconstruction tool.

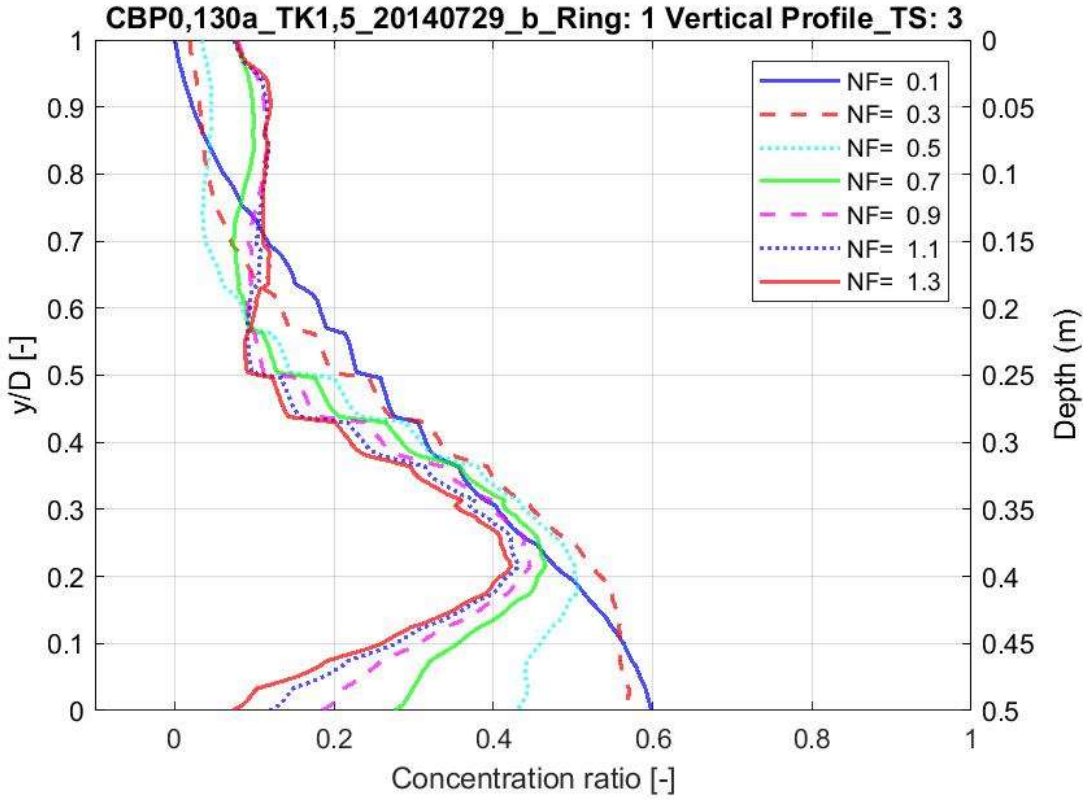

Figure 4.9 Test CBP0,130a_TK1,5_20140729_b. Results for the same file between different NF values.

For so, a Fixed Noise Figure of 0.2 is selected for the results later presented in this dissertation and the target elements to set the contrast of this chosen Noise Figure are set in the elements going from the 450 to the 454 out of 576 elements.

c. *Background conductivity*

Background conductivity generates the different contrasts of the images processed. As ERT detects changes in the conductivity with respect the background, it is important to set an appropriate value for the background conductivity so that proportional differences and equal values are obtained in each of the images of the same test.

To prove the effect of the background conductivity, this parameter is tested out by doing iterations in the calculus of the same tomographic measurements with different background conductivity levels ranging from 0.1 to a maximum of 2 increasing at each step the 50% of the previous value. Some of the results obtained in this sensitivity analysis are shown in Figure 4.10. In this figure, same image is shown but different range of values are obtained so that in a colour scale between 0 and 1 the visualization does not look like the same since depending on the values of the background different range of values for the elements of the circular mesh are obtained.

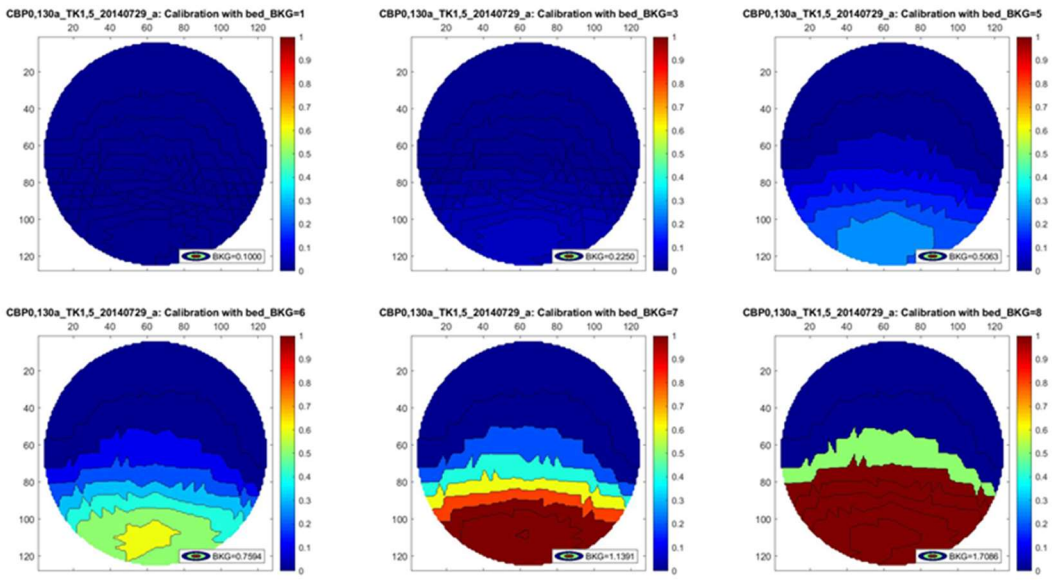

Figure 4.10 Test CBP0,130a_TK1,5_20140729_a. Some representative values obtained for the calibration bed depending on the background value set.

The contrast obtained in the images changes with respect the definition of the background conductivity. Background conductivity sets the rank for the values inside an image but, since every measurement corresponds to an image, it is important to stablish the same scale for the values in all the images of the same test by correctly introducing the background conductivity calculated in every measurement, so that the later concentration values obtained in the processing are realistic and the relation between their values keeps being proportionate to the concentration.

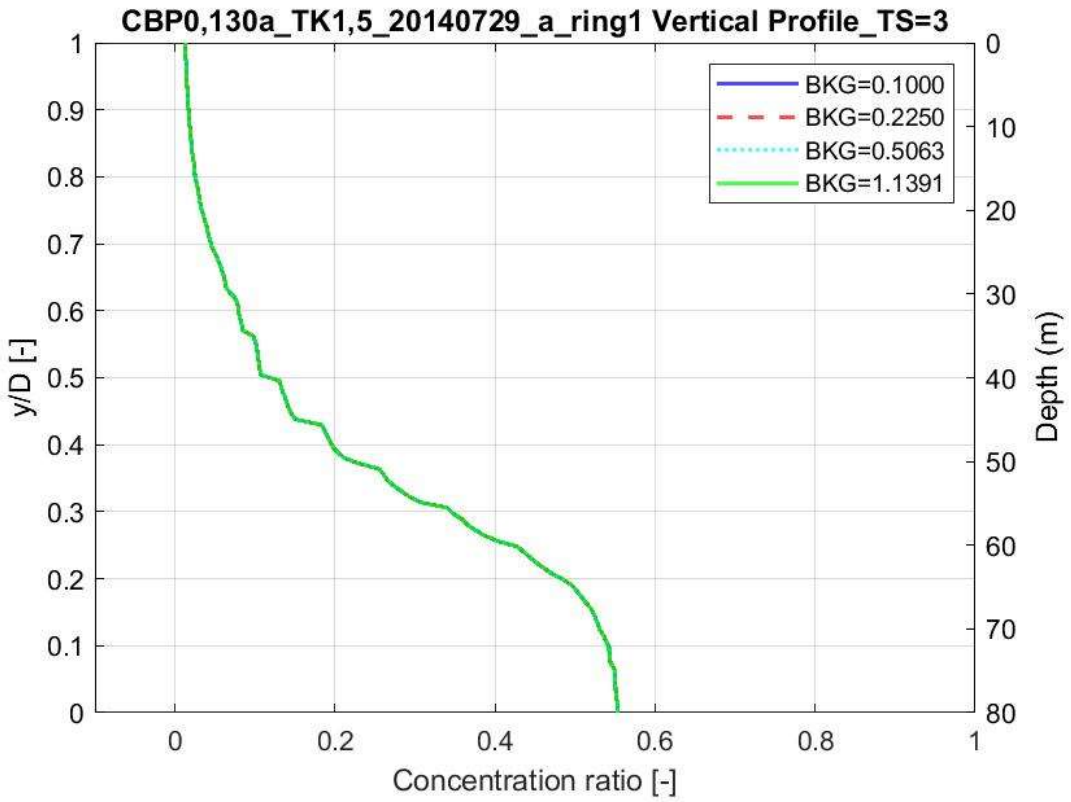

Figure 4.11 Test CBP0,130a_TK1,5_20140729_a. Vertical profile obtained in Ring 1 measurement 3 for different background values.

In fact, it has been shown that for this different background values when they are established for the entire compendium of measurements of a test, the same profile for each one of the measurement in the test is obtained independently of this conductivity value introduced (Figure 4.11), since concentrations are lineal interpolations depending on this values.

On the other hand, it has to be taken into account the unique background value of each image as usually conductivity appears to have small changes during the process due to the energy dissipation of the flow into heating energy, which will at the same time change the temperature and then the electrical conductivity of the mixture. Consequently, to keep the real scale between different measurements it is important to fix their real background conductivity value in each of them.

In this sensitivity analysis it is also shown that the maximum and minimum value in the same calibration file it's not the same depending on the background conductivity set, as it can be seen qualitatively in Figure 4.10 and numerically in Figure 4.12.

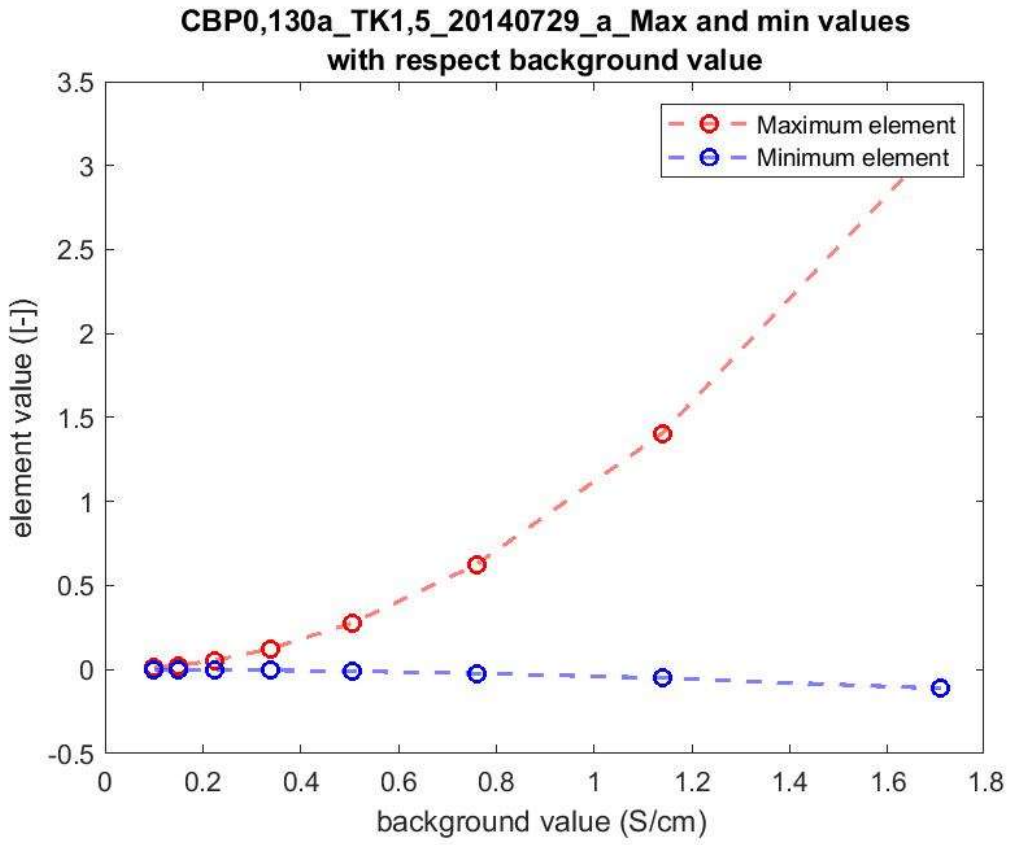

Figure 4.12 Test CBP0,130a_TK1,5_20140729_a. Maximum and minimum values obtained for the same calibration files depending on the background conductivity set.

Nonetheless, it is known that not all measurements in the set are done with exactly the same conductivity. For so, it can be concluded that the contrasts of the images are proportionate to the background value and, as a deduction, it is important to correctly set this background value in each one of the measurements done. In order to keep the real proportion between them.

Since the only known values for each test are the background conductivity at the calibration measurement and before and after the test is carried out, the background is considered for each one of the measurements of the test a linear interpolation between the starting and the final value for this conductivity and the number of tests done.

.

4.1.2 2D concentrations

2D images show the whole cross-section image for the three of the rings set in the pipeline. This images also help to give a non-numerical interpretation of the results and so a non-technical overview of them. Thus, from the 2D images the evolution of the concentration of the rings is shown in a not technical way to interpret, and it is possible to see the characteristics of the flow without any supporting numerical data.

This 2D images can be obtained, initially, for the post-processing values of the image after the EIDORS treatment and, later in the script, with escalated values as a representation of the interpolated concentrations. Both of them, look similar although the scale of the colours may vary since values are also escalated for the concentrations.

In all tests carried out it can be appreciated the effect of the pipe elbow of this fluid-solid circuit, since the last of the rings (Ring 3) images have skewed beds (Figure 4.13). For this reason, the third ring values obtained in this work are not considered as representative values in the analysis of the results, as the effect of this distorted values would affect also in the calculation of the chord-average and median in the 1D concentration distribution profiles, not giving realistic values neither trends (smoothing the average as there is more variability of values, less robustness), and so misleading to non-realistic values.

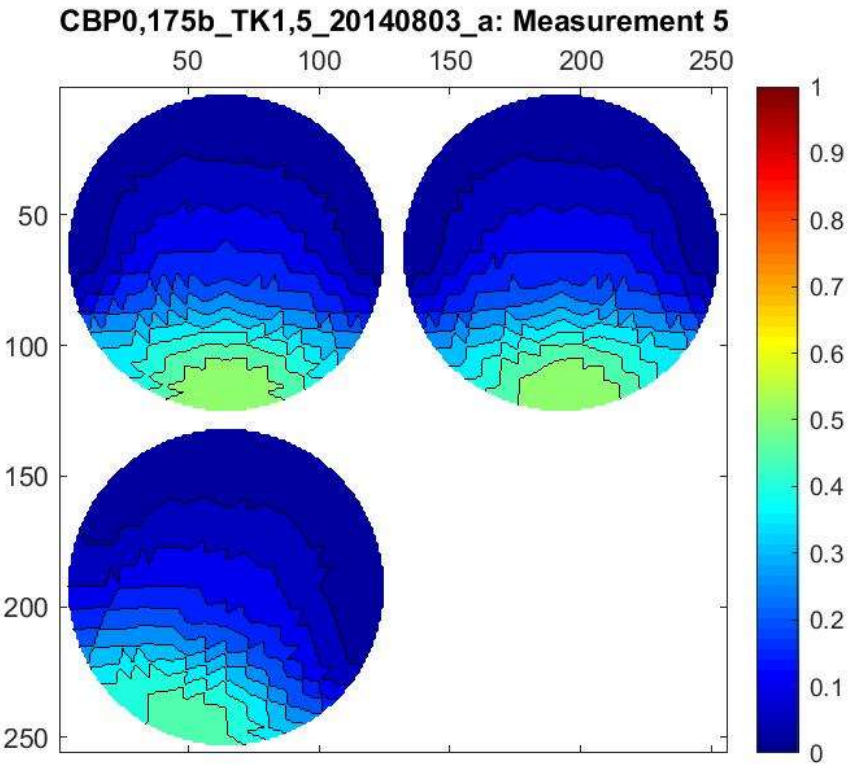

Figure 4.13 Test CBP0,175b_TK1,5_20140803_a : 2D image after EIDORS post-processing, for the measurement 5 in the 3 rings.

For lower velocities of the tests, a bed in the bottom of the pipe can be observed in the images reconstruction. It is in this part of the tests where higher concentrations are obtained. In this plots, it is possible to appreciate the stratified flow and distinguish between a layer of particles in the bottom, where the maximum local concentrations are achieved, and another layer on the top of the pipe with the fluid flowing where almost null concentrations are obtained (Figure 4.14, top row).

On the other hand, when velocities increase, the bed tends to disappear and a mixture between the particles and the Carbopol appears. The distribution in the cross section of the particles gets more and more homogeneous as it can be appreciated in images where there is almost the same colour (value) all over the inside of the pipe. Therefore, in this images the maximum local concentrations obtained are lower than in higher velocities measurements done in each test. This behaviour described can be seen in the figure below this lines (Figure 4.14, bottom row).

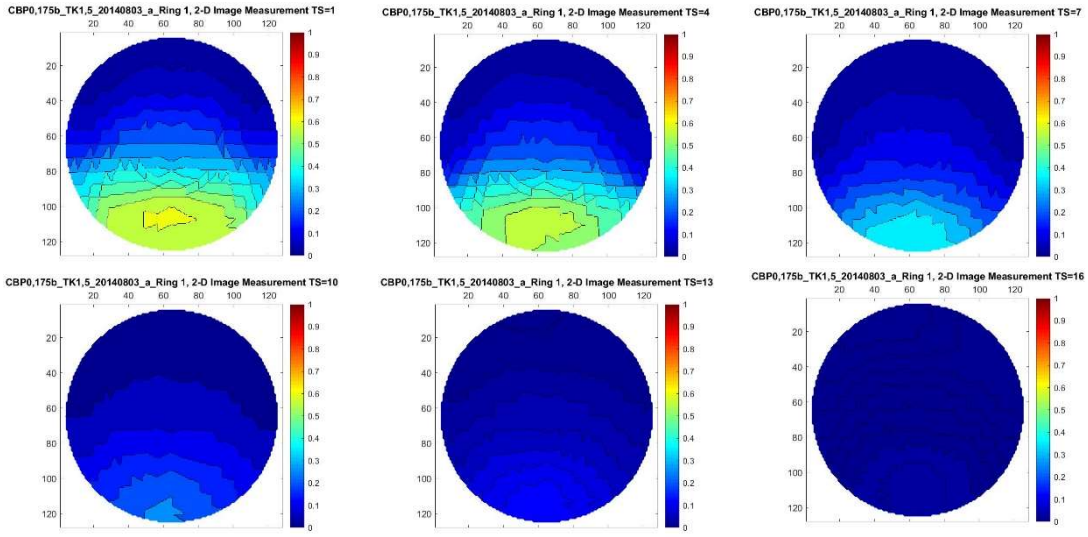

Figure 4.14 Test CBP0,175b_TK1,5_20140803_a, Ring 1. Evolution of the 2D images for the concentrations obtained in the pipe.

4.1.3 1D concentration profiles

The 1D concentration profile is obtained from a chord-average through every row of the matrix containing the values of the firstly interpolated concentration seen in the 2D images. It appears to be the concentration distribution along the vertical axis of a specific cross-section inside the pipe. To check the robustness of this chord-average results, also the median of the concentration values is calculated and plotted (Figure 4.15).

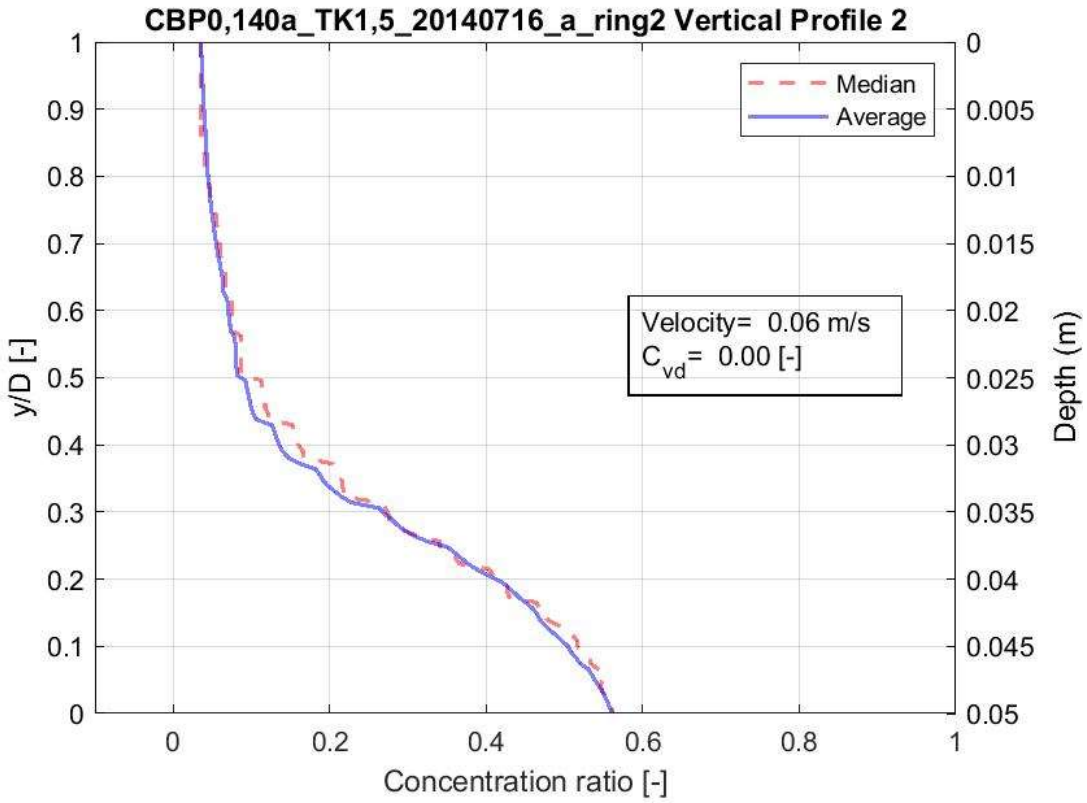

Figure 4.15 Test CBP0,140a_TK1,5_20140716_a, Ring 2, measurement 2. 1D 1D concentration profile.

For all the tests done in this work, the trends look similar along the changes on the velocity and the delivered concentration given, but the values are slightly displaced to the left and to the right (smaller and greater concentration), depending on the maximum and minimum values obtained during the initial calibration and then updated during the running of the computational tool with the recalibration introduced.

When lower velocities are given, distribution usually has a vertical logarithm shape. This situation occurs in the beginning of the tests measurements. For all the tests processed, this shape for low velocity profiles matches with the real distribution of the particles seen in the video images (Figure 4.16).

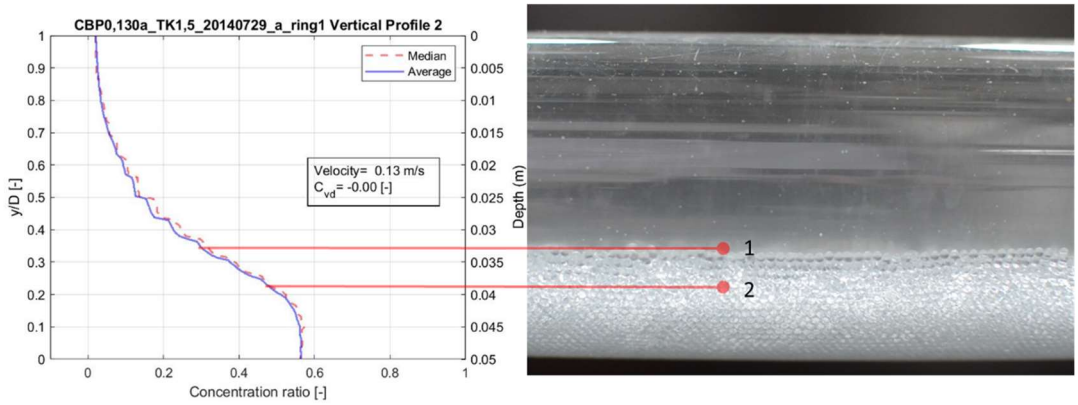

Figure 4.16 Test CBP0,130a_TK1,5_20140729_a, Ring 1, measurement 2. Comparison between the video images and the 1D profile obtained.

As it can be seen in Figure 4.16, from the top of the figure until point 1, concentration is almost null and increases in a very slow range. In point 1 the maximum steepness for the concentration is reached as the movable (less dense) bed appears. Where, from point 2 in the image until the bottom of the pipe, the fixed bed is achieved so there is no change in the concentration and the values in this part of the profile are around the 60% (0.6) set as the maximum concentration.

On the other hand, as the velocities and delivered concentration are increased, the distribution curve of the particles tends to turn into a vertical lineal shape, since a more uniform distribution of the particles inside the pipe takes place (Figure 4.17). This part of the flow is more difficult to capture not only for ERT but for the video images. And, it is the part more sensible to be post-processed for two different related reasons. First, because Carbopol is changing properties so that conductivity may vary with respect the initial calibrations and, subsequently because, since this values are closer to the 0 concentration value, the measurement error is higher penalised when calculating the concentration.

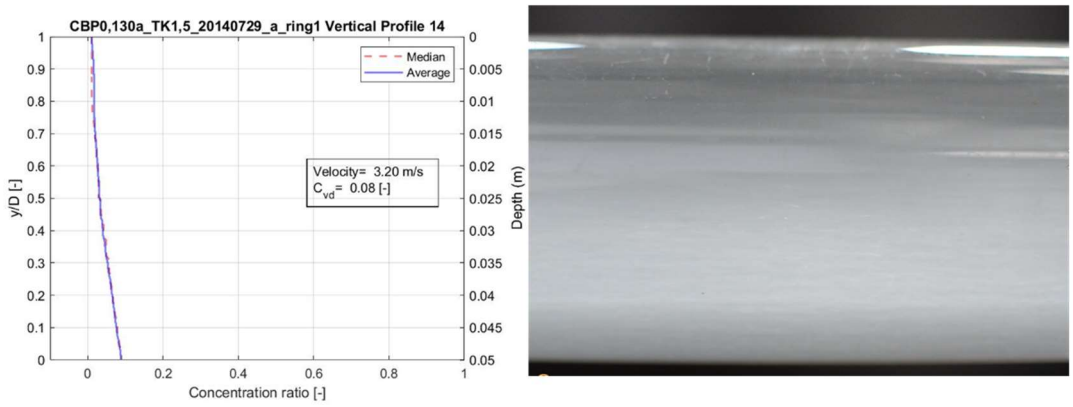

Figure 4.17 Test CBP0,130a_TK1,5_20140729_a, Ring 1 measurement 4. Comparison between the video images and the 1D profile obtained.

The general evolution of the profiles is shown in the below figure, where all the transition profiles between Figure 4.16, representing a fully stratified flow, to Figure 4.17, showing an quasi homogeneous flow, can be appreciated in the figure below Figure 4.18.

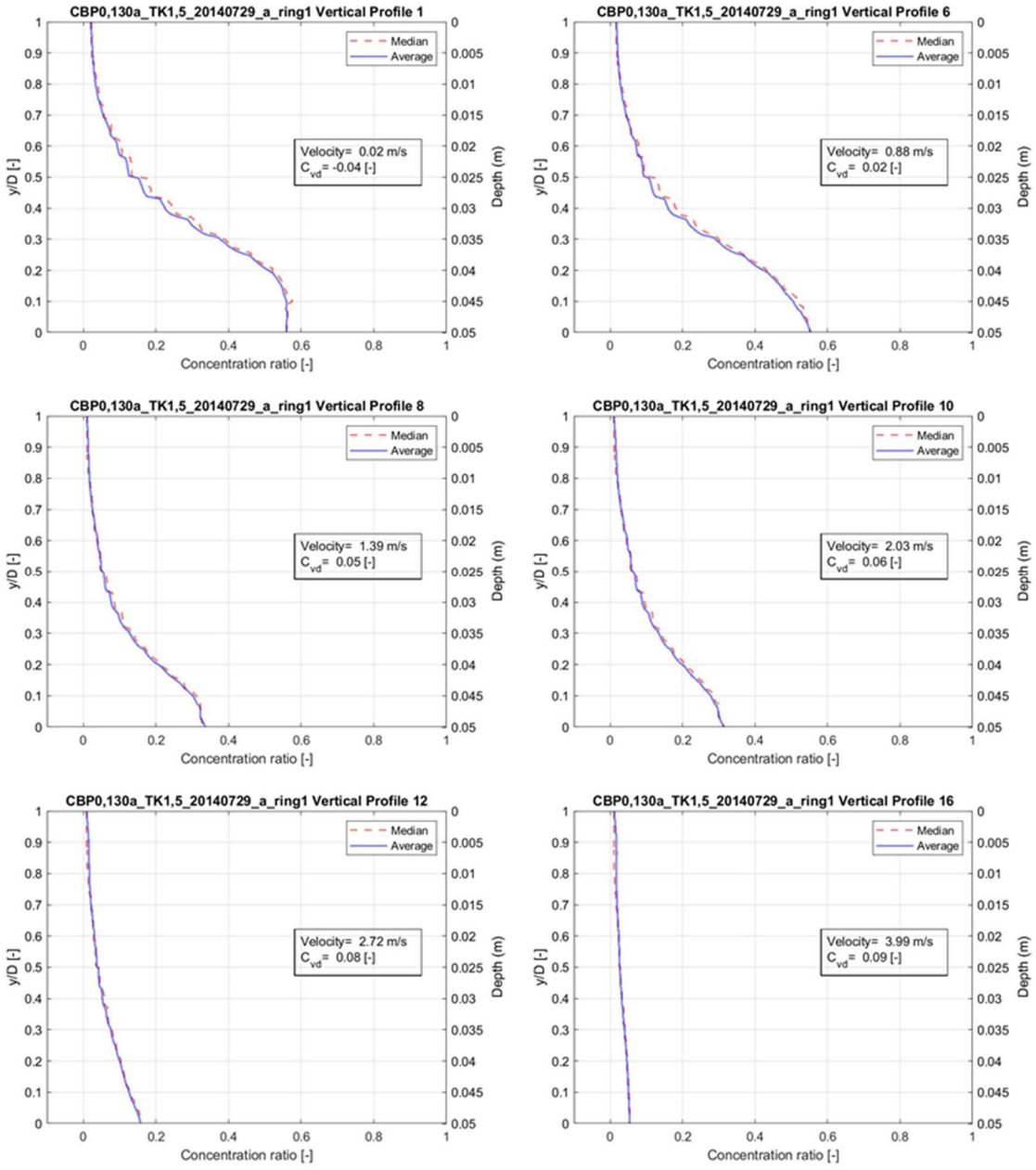

Figure 4.18 Test CBP0,130a_TK1,5_20140729_a, Ring 1. Evolution of the profiles obtained during the measurements.

Differences between the rings in the same measurement may be also appreciated. For the third ring, since it is placed the last from the direction flow point of view it is the nearest to the elbow of the closed circuit and thus, the particles bed is usually skewed because it can notice the change on the direction of the flow. Since there is a distortion of the perpendicular axis with respect the bed, the chord-average done for every layer of this bed includes a wider range of values and usually it has a smoother change in the values, more tended curves. In ring 1 usually, the highest local concentrations are obtained since it is the one placed in the beginning of the loop circuit, so concentrations are reached faster (Figure 4.19).

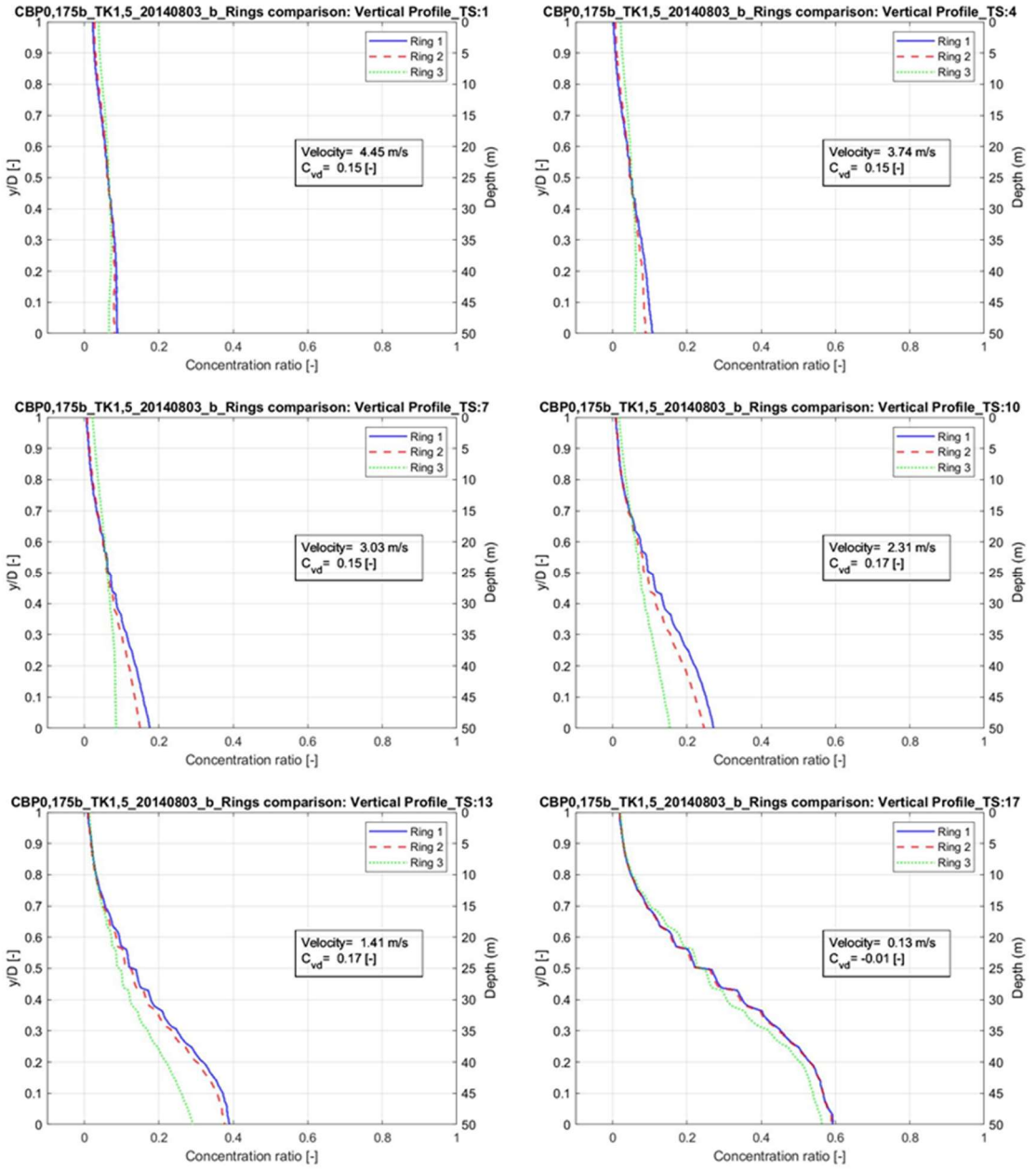

Figure 4.19 CBP0,175b_TK1,5_20140803_b. Comparison between rings evolution.

4.1.4 Average concentrations

The average concentration depends exclusively on the integration of the 1D concentration profile. Therefore, the values obtain certainly are subject to the accuracy of the values obtained in the 1D concentration profiles. As it has been seen in the previous section, linear profiles for all the test follow the same behaviour during the measurement depending on the velocity. On the other hand, although following the same pattern, the values may not be as precise as wanted in all the cases, so the magnitude of the error in the values for the 1D profiles gets increased when calculating the C_{vi}.

While in the tests the delivered concentration (C_{vd}) is increasing with the velocity, the in situ average concentration calculated with the computation tool (C_{vi}) is expected to drop. Theoretically, the delivered and the in situ calculated concentration should converge to the same value as velocity increases, meaning that they both reach an equilibrium ($C_{vd} \approx C_{vi}$).

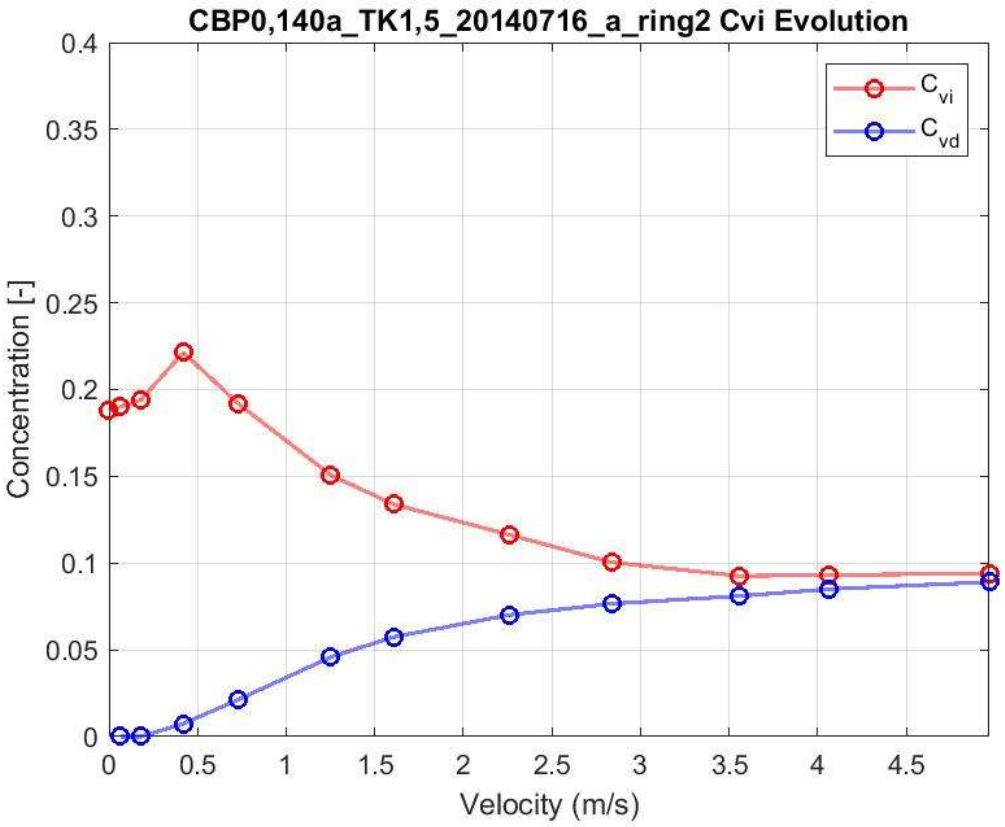

Figure 4.20 CBP0,140a_TK1,5_20140723_a, ring 2. Evolution of the delivered and measured average concentrations depending on the velocity (C_{vd} and C_{vi} respectively).

As seen in Figure 4.20, trends for all of the test done are having the behaviour expected, although some points can get some error variance error because of the static interpretation of the flow, which in fact is not steady.

Almost all of the tests, from lower to a middle range velocity it can be appreciated how both concentrations are converging as expected. However, for high velocities are usually having values lower than the ones obtained the calibration file with solely Carbopol, and although the recalibration has been included, even with it, the integration of this high velocity profiles usually decreases to smaller values than expected instead of maintaining a steady number. This may be explained because the 0% concentration set during the calibration corresponds to the value of some point in the image and, regardless of being more adjusted than the initial 0 concentration of the calibration file, it is still not a perfect measurement and it may include the effect of some particles.

Nevertheless, this impediment may be overcome by the improving in the tune up of the computational tool regarding an enhanced definition of the Carbopol rheological properties or/and an enhancement in the quality of the image results by a more defined parametrisation in EIDORS.

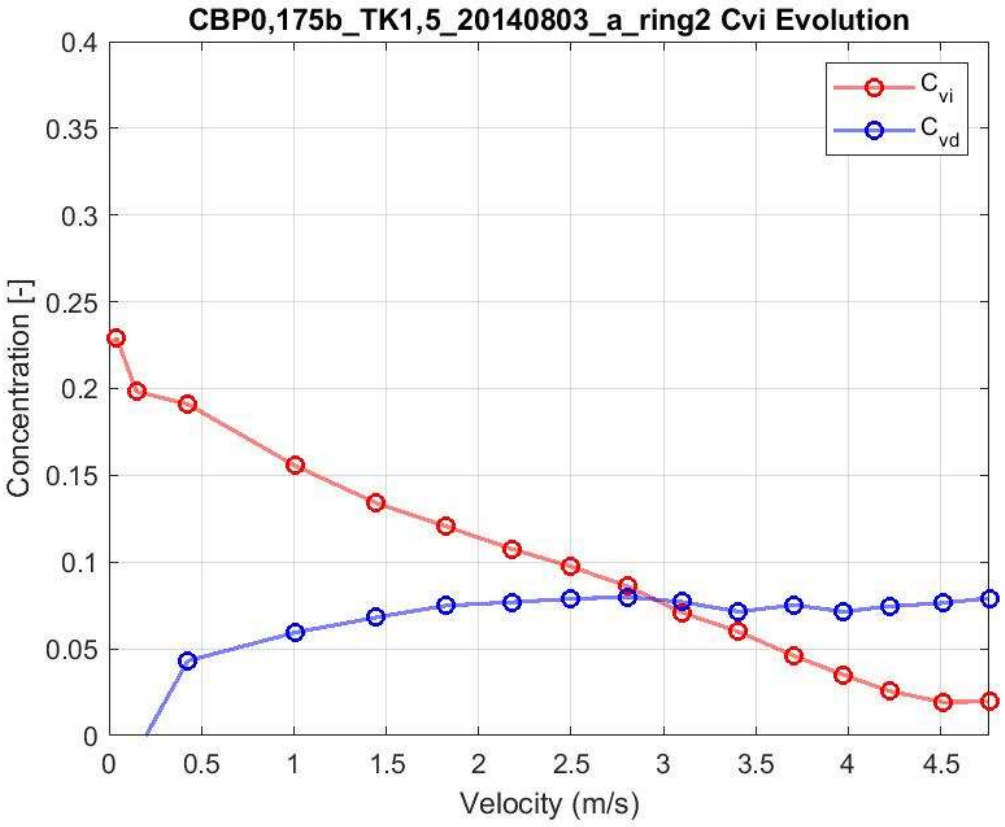

Figure 4.21 CBP0,175b_TK1,5_20140803_a Ring2. Evolution of the delivered and measured average concentrations depending on the velocity (C_{vd} and C_{vi} respectively).

4.2 Analysis of water-based slurry

A test with slurry based on water carrier is also computed by the computational tool develop with the purpose of checking its effectiveness with a more stable fluid than Carbopol. Using the same script for water the results obtained are much more accurate than for the Carbopol ones. For the 1D concentration profiles the same trend as for Carbopol are presented as it can be seen in the following figure (Figure 4.22): for higher velocities distribution tends to be more vertical while decreasing the velocity the profiles turn out to a more tended logarithmic curve.

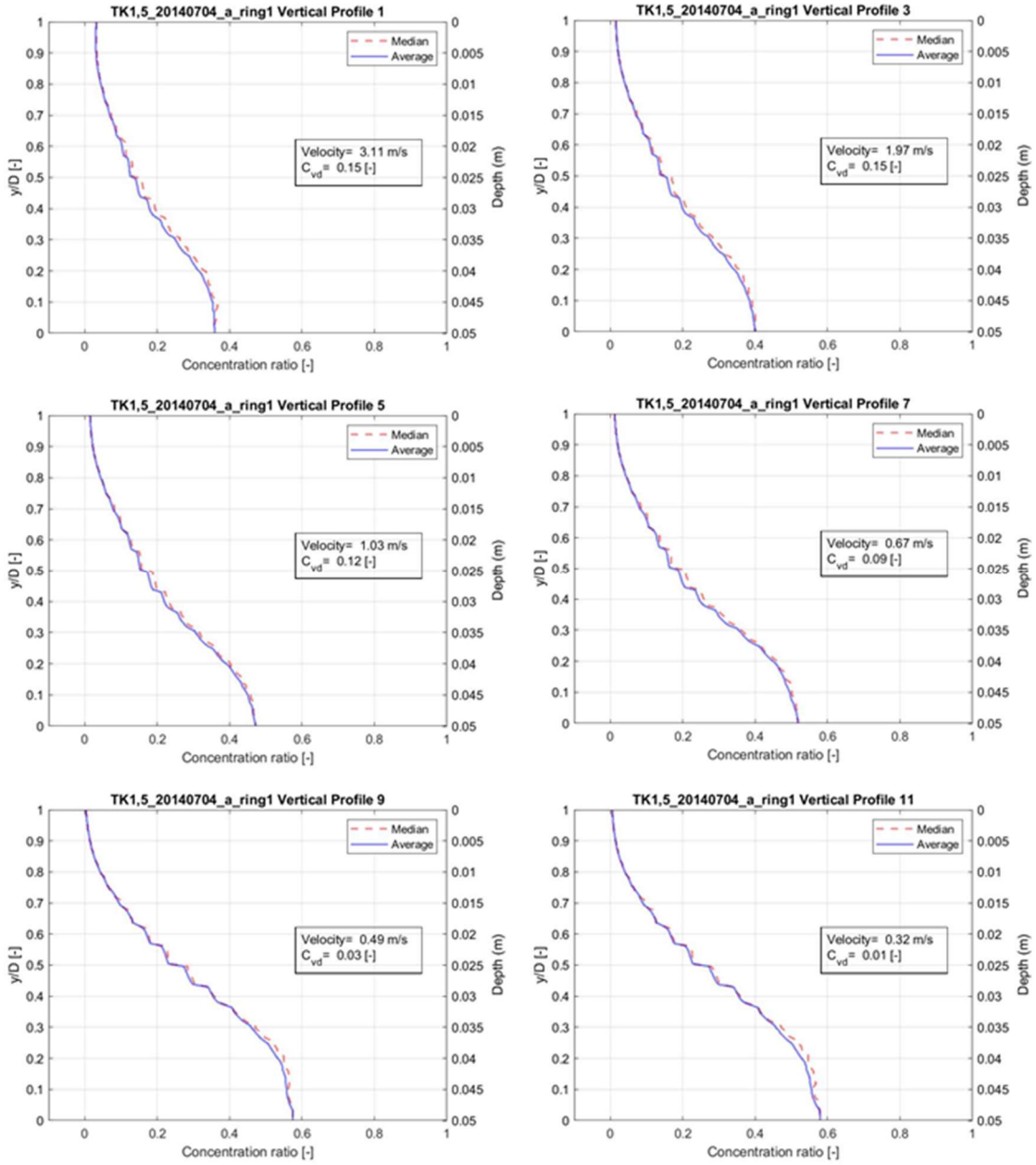

Figure 4.22 Test waterTK1,5_20140704_a. Evolution of the profiles obtained during the measurements.

For the average concentration, in the case of water it can be observed that for neither of the rings a lower C_{vi} is measured with respect to the corresponding C_{vd}. The shape of the graphics is always convergent as expected.

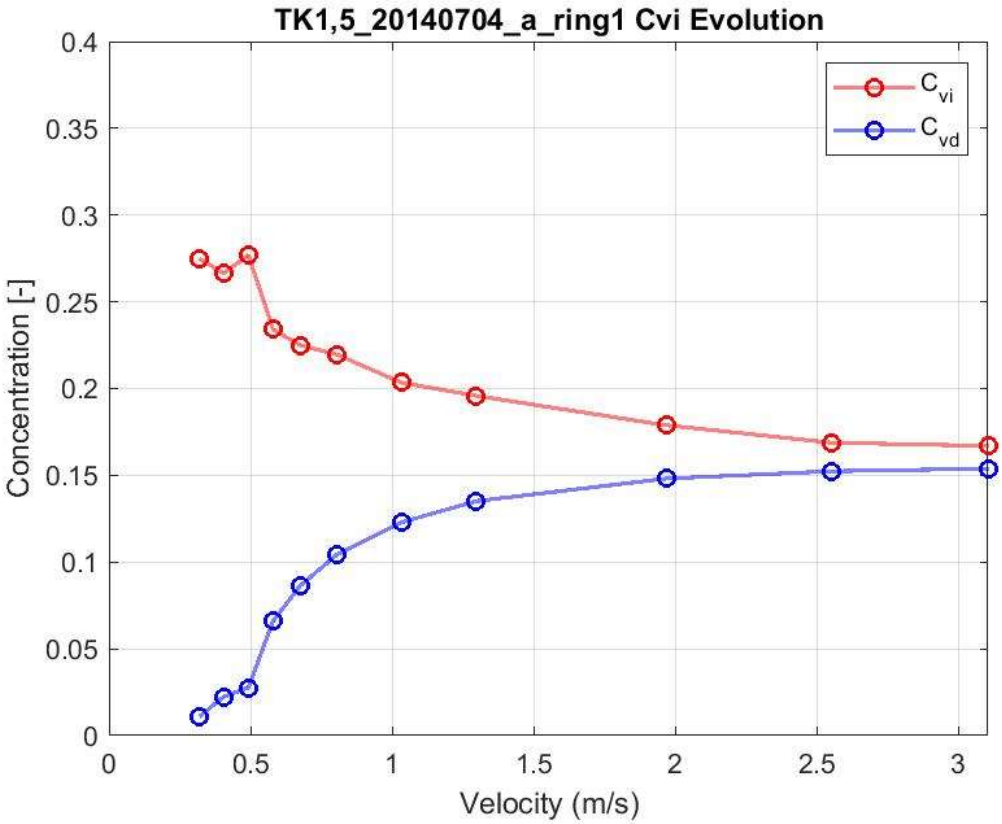

Figure 4.23 Test waterTK1,5_20140704_a, ring 1. Evolution of the delivered and measured average concentrations depending on the velocity (C_{vd} and C_{vi} respectively).

This confirms that the tool created with EIDORS, the set up done for the adequate visualisation and the further scripts for the analysis are working as expected, and gives a hint for further progress which may be mostly related with a better characterisation of the Carbopol, since for water the results obtained are correct.

Chapter 5. Conclusions

To summarize, the results obtained within the developed script are in the right path, the trends perfectly describe the behaviour expected and provide useful information of the behaviour of the solid-liquid mixture. For lower velocities a stratified flow is obtained while in the higher velocities it is possible to appreciate homogeneity for the cross-section in all of the results. Trends in the average concentration always show a decrease in concentrations from lower to higher velocity. Besides, some more accuracy in the numerical values could be achieved with further development in the code. Nevertheless, the results might be useful to support and contrast a physical model to interpret the behaviour of a slurry pipeline. Therefore, the main goal can be considered to be accomplished.

From a global point of view, the tool is working with effectiveness, rapidly and gives promising results to use in the study of the two-phase mixture with a non-Newtonian fluid. With further adjustment of the script, ERT might turn out to be a very powerful tool, for the different advantages that supposes over other techniques in the slurry pipelines field. For the ratification of the goodwill of the program, not only a mixture with a non-Newtonian fluid but with water is tested out and it can be concluded that the expected behaviour is obtained.

As one of the limitations, it has to be kept in mind that, since Carbopol is much more unstable than water (and for so its properties keep changing while the measurements are carried out) trying to obtain clear profiles still has a future way to go. In other words, Carbopol properties need to be defined in a more detailed way in order to obtain the same precision than in the case of a Newtonian liquid. Moreover, the analysis done supposes in both cases, for water and Carbopol, a stable flow (“instant photo”), and even for water, that is not changing properties itself, turbulent flow is not a steady state. So, in any case, it cannot be pictured with perfect detail the real flow, but it is a very good approximation. In fact, this is a limitation of the ERT technique itself and, even through it, results, especially in water, are very close to the expected theoretical ones.

It is noticeable that the results depend on the appropriate methodologies followed both for the measurement and for the post-processing. Setting a good calibration of the measurements shows to have big effect in the final values for the different concentrations obtained in the post-processing. A very poor adjustment in the calibration can lead to mistaken concentrations. In order to try to fix this measurement mistakes, a recalibration is set during the processing. In the criteria analysis is seen that, for each test, its own calibration file plus the recalibration of the maximum and the minimum concentrations during the post-processing gives the most fitting results for the data analysed. This modification of the code, including the recalibration, avoids negative values and values over the maximum possible concentration, but it still can be improved by having a better rheological

characterization of the Carbopol relating it with velocity and temperatures obtained which, by now, is not directly taken into account in the post-processing. It is also suggested to obtain for the calibration values for solely Carbopol flow (with different velocities. With it some of the lower concentrations obtained for the higher velocities may be upgraded, as there would be a calibration file for 0% concentration of Carbopol at each one of the measurements.

As more manipulation is done into the results, the accumulated error keeps increasing, meaning that, local 1D concentration profiles are more reliable than the average concentration since it is an integration of this 1D profiles. For this integration, trapezoidal method has been imposed in the computational model for its tested performance in other works. However, trapezoidal method does not take into account the circular shape of the pipe.

Also, with respect to the methods of the processing of the files, it is seen that it is quite difficult to set objectively the visualization of the images. EIDORS gives the possibility to post-process the images, but this images are really sensitive to the parametrization done and its trustworthiness must be supported by other variables obtained with other techniques or previously known. In this work the direct setting of the parameters by the user is introduced in the code instead of using the default configuration of EIDORS. Regarding this parameters, hyperparameter value is the most defining one in the reconstruction of the image to obtain appropriate results. Fixed Noise Figure method has been introduced in the scripts for the selection of the hyperparameter. This method avoids the necessity to find out manually the best hyperparameter for each one of the post-process of the measurements. In the analysis criteria it is determined that the most fitting results are obtained when using a Noise Figure between 0.2 and 0.3 for all the tests carried out in this work. Also, in this hyperparameter analysis it can be seen that values obtained near the wall of the pipe are usually lower even when there is a bed concentration. That can be explained because of the influence of the electrical currents injected, meaning an instrumentation error and, if corrected, values may be better fitting.

It is also important to take into account the background conductivity. As concluded, background conductivity scales the visualization values and has to be appropriately stablished for all the measurements in one set to correlate values between each other. It is evidenced to be important to initially set this background conductivity for all of the files. Right now, the computational model is using a lineal relation between the starting background conductivity and the final background conductivity to set a conductivity at each measurement. This procedure of setting a background value could be enhanced with more data about the evolution of the conductivity during the measurements.

Regarding the final results obtained, having a look at the 1D concentration profiles the shape of the functions obtained with the use of their own calibration and the recalibration method usually look good and concentrations seem adequate if they are compared to the video images, especially for lower velocities. With higher velocities where all the materials are suspended it becomes much more difficult to define the real concentration. Henceforth, for the average concentration the trends have the expected behaviour but values usually don't converge with the delivered concentration when higher velocities are given. In most of the cases the asymptote expected for the C_{vi} when it reaches higher velocities is lower than the delivered concentration value (C_{vd}), when, in fact, there should be seen a convergence between both values. Some of the possible improvements mentioned before for the calibration and parametrization of the scripts may correct this mistake.

In conclusion, it is believed that results are going in the right path and give a general idea of the behaviour but it is also important to notice that there is still work to do in this field in order to better characterize the two-phase flow for a non-Newtonian fluid solely with the ERT technique.

5.1 Recommendations

As said, the progression in the definition of the Carbopol rheological properties and its inclusion in the computational model may be key future lines for the project to develop. It is suggested to try to obtain calibration files for solely Carbopol flow, meaning that values for clear Carbopol at a certain velocity and current value are measured and can be set as new recalibrations of the model at each time step instead of using values found in the measurement files themselves for the recalibration. This, is thought, will provide better results in the obtaining of concentrations and better convergence in the graphs for the average concentrations.

Also, more exhaustive information regarding some of the parameters would be good for the better adjustment of the program, i.e. for the background conductivity it would be good to obtain its values at each time step. Moreover, collecting some extra data in the measurements, for example temperature at each time step, may also help in the definition of the Carbopol.

Regarding the scripts used and the parametrization of EIDORS it is noticed that in the walls of the pipe the influence of the current emission by the conductive electrodes is noticed by a decrease in the concentrations. A correction of the images for the presence of the wall which avoided the effect of the presence of the emission electrodes, would also be considered as a future way.

Finally, regarding the integration, it is also suggested to develop or include an integration method taking into account the circular shape of the pipe.

References

Adler, A., & Guardo, R. (1996, 04). Electrical impedance tomography: regularized imaging and contrast detection. *IEEE Transactions on Medical Imaging*, 170-179. doi:10.1109/42.491418

Adler, A., & Lionheart, W. R. (2006). Uses and abuses of EIDORS: an extensible software base for EIT. *Physiological Measurement, 27*(5). doi:10.1088/0967-3334/27/5/s03

Banner Engineering. (n.d.). *Banner Engineering.* Retrieved from Detecting Leaks Along a Coal Slurry Pipeline: https://www.bannerengineering.com/in/en/solutions/other/detecting-leaks-along-a-coal-slurry-pipeline.img.png

CFD support. (n.d.). Laminar flow with ggplot2 and gganimate. Retrieved from https://eugejjoh.files.wordpress.com/2018/04/sketch-laminar-flow-turbulent-flow.png?w=300&h=274

Dickin, F., & Wang, M. (1996). Electrical resistance tomography for process applications. *Measurement Science and Technology*, 247-260. doi:10.1088/0957-0233/7/3/005

Graham, B. M., & Adler, A. (2006). Objective selection of hyperparameter for EIT. *Physiological Measurement, 27*(5). doi:10.1088/0967-3334/27/5/s06

Grychtol, B., & Adler, A. (2013). Uniform background assumption produces misleading lung EIT images. *Physiological Measurement, 34*(6), 579-593. doi:DOI

Itoms. (n.d.). *ITS (Industrial Tomography System).* Retrieved from Slurry flows: https://www.itoms.com/wp-content/uploads/2013/06/slurry-flow-individual.jpg

Kesely, M. (2016). Evaluation of settling velocity of coarse particles in visco-plastic fluid and frictional loss in complex slurry flow. Prague.

Kesely, M., & Matoušek, V. (2016). Laminar Settling Of Glass Beads In Visco-Plastic Liquids. *Stavební obzor - Civil Engineering Journal*. doi:10.14311/cej.2016.01.0001

Pang, J., & Cheung, G. (2017, 08 12). *Graph Laplacian Regularization for Image Denoising: Analysis in the Continuous Domain.* Retrieved 2018

Peník, V., Kesely, M., & Matoušek, V. (2016). Coarse particle support in turbulent flow of visco-plastic carrier. *EPJ Web of Conferences*, *114.* doi:10.1051/epjconf/201611402090

Ramsdell, R., & Miedema, S. (2007). An overview of flow regimes describing slurry transport. *18th World Dredging Congress 2007.*

Rheology of Drilling Muds. (n.d.). Retrieved from http://rishibabuadari.tripod.com/MudRheology/Rheology.htm

Samorè, A., Guermandi, M., Placati, S., & Guerrieri, R. (2017). Parametric Detection and Classification of Compact Conductivity Contrasts With Electrical Impedance Tomography. *IEEE Transactions on Instrumentation and Measurement, 66*(10), 2666-2679. doi:10.1109/tim.2017.2711818

Sharifi, M., & Brent, Y. (2013). Electrical Resistance Tomography (ERT) applications to Chemical Engineering. *Chemical Engineering Research and Design, 91*(9), 1625-1645. doi:10.1016/j.cherd.2013.05.026

TU Delft OpenCourseWare. (2018). *TU Delft OCW.* Retrieved 2018, from 3. Flow of mixture in a pipeline: https://ocw.tudelft.nl/course-readings/flow-of-mixture-in-a-pipeline/?course_id=786

Vauhkonen, M., Lionheart, W., Heikkinen, L., Vauhkonen, P., & Kaipio, J. (2001). A MATLAB package for the EIDORS project to reconstruct two-dimensional EIT images. *Physiological Measurement, 22*, 107-111. doi:10.1088/0967-3334/22/1/314

Wilkinson, A. J., Randall, E. W., Long, T. M., & Collins, A. (2006). The design of an ERT system for 3D data acquisition and a quantitative evaluation of its performance. *Measurement Science and Technology*, 2088-2096. doi:10.1088/0957-0233/17/8/006